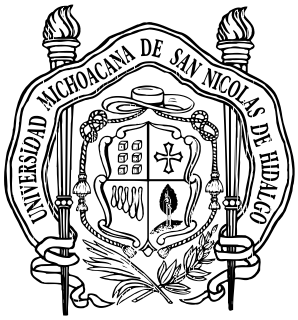

UNIVERSIDAD MICHOACANA DE SAN NICOLÁS DE HIDALGO

FACULTAD DE INGENIERÍA ELÉCTRICA
DIVISIÓN DE ESTUDIOS DE POSGRADO

Steady-State model of grid connected photovoltaic generation for power flow analysis and grid code requirements

by

Rafael Tapia Juárez

A thesis submitted in fulfilment of the requirements

for the degree of

Doctor of Science in Electrical Engineering

Directora de Tesis

Dra. Elisa Espinosa Juárez

Co-Director de Tesis

Dr. Claudio Rubén Fuerte Esquivel

MORELIA, MICHOACÁN Febrero 2019

STEADY STATE MODEL OF GRID CONNECTED PHOTOVOLTAIC GENERATION FOR POWER ANALYSIS AND GRID CODE REQUIREMENTS

Los Miembros del Jurado de Examen de Grado aprueban la **Tesis de Doctorado en Ciencias en Ingeniería Eléctrica, Opción en Sistemas Eléctricos** de ***Rafael Tapia Juárez***

Dr. J. Jesús Rico Melgoza
Presidente del Jurado

Dra. Elisa Espinosa Juárez
Director de Tesis

Dr. Claudio Rubén Fuerte Esquivel
Co-director

Dr. J. Aurelio Medina Rios
Vocal

Dr. Salvador Acha Daza
Revisor Externo (Centro Nacional de Control de Energía)

Dr. Juan Anzurez Marín
Director de la Facultad de Ingeniería Eléctrica. UMSNH
(Por reconocimiento de firmas)

UNIVERSIDAD MICHOACANA DE SAN NICOLÁS DE HIDALGO
Febrero 2019

To my parents Elena and Rafael Sr. for their unconditional love...

Abstract

A new model of a grid-connected photovoltaic (PV) plant suitable for power flow analysis is proposed in this thesis. Unlike existing models, the proposal departs from the equivalent generator representation of the PV plant and is based instead on the operation and control modes of PV panels and voltage source converters (VSC). The resulting set of nonlinear equations is assembled together with the network's equations to formulate a generalized power flow problem in a unified frame of reference, which is efficiently solved by using the Newton-Raphson algorithm. The complementarity condition approach is adopted for directly including all operation and control mode constraints of the PV plant in the power flow formulation, which permits the simultaneous and automatic handling of limits of all state variables associated with these constraints during the iterative solution process. This also makes it possible to consider the technical requirements established in grid codes for the interconnection of asynchronous generation to the electrical system; in particular, requirements established in the Mexican Grid Code have been included. The effectiveness of the proposed method is fully demonstrated by numerical examples.

Resumen

En esta tesis se propone un nuevo y novedoso modelo de una Planta Fotovoltaica que tiene por objetivo principal el análisis en el problema de flujos de potencia. A diferencia de los modelos existentes, esta propuesta no es considerada como un modelo de generador equivalente, en cambio, se basa fielmente en los modos de control de los generadores PV y su convertidor asociado. El conjunto resultante de ecuaciones no lineales es acoplado con las ecuaciones que describen la red para formular un problema de flujos de potencia generalizado en un marco de referencia unificado, el cual es eficientemente resuelto usando un algoritmo Newton-Raphson. Se toma en cuenta un enfoque de condiciones de complementariedad para incluir todas las restricciones de operación de la Planta Fotovoltaica en la formulación del problema de flujos de potencia, lo que permite un manejo simultáneo y automático de los límites de todas las variables de estado asociadas a estas restricciones durante el proceso iterativo de solución. Esto permite además, considerar los requisitos técnicos establecidos en códigos de red para la interconexión de generación asíncrona a la red eléctrica; en particular, se han incluido los requerimientos establecidos en el Código de Red de México. La efectividad del método propuesto es demostrado con simulaciones y ejemplos númericos.

Palabras clave: Planta Fotovoltaica, Flujos de potencia, restricciones de operación, algoritmo Newton-Raphson, generación asíncrona

Acknowledgements

First, I would like to express my sincere gratitude to my co-advisor and mentor Prof. Claudio Fuerte for the continuous support of my research, for his motivation and guidance throughout these years. I am deeply greateful with him, not only for giving me the opportunity to work under his supervision, but must important for his contributions and valuable suggestions in my research as well as his advice in my daily life.

I would also like to acknowledge to my advisor PhD. Elisa Espinosa for offering me the opportunity to study my PhD and for the contributions and discussions throughout these years. I would also thank to the esteemed commited members: PhD. Salvador Acha, PhD. Aurelio Medina and PhD. Jesus Rico for the valuable input that they have given into my thesis.

I like to thank Consejo Nacional de Ciencia y Tecnología (CONACYT) of México fo the financial support during my doctoral study.

My warmest thanks from the bottom of my heart to my parents Elena Juárez and Rafael Tapia Sr. for give me the best education and always look after me. I dedicate this thesis to them, for their endless support. I gretaful to my sister Melissa for her encouragement.

I also extended a very special acknowledgement to América who supported me throughout this PhD. path, thank you for always belive in me.

Last but not the least, I want to thank my friends, MSc Uriel Sandoval for his constructive suggestions in this thesis and continuous motivation. PhD R. Rodrigo and MSc Julio Raya who always willing to clarify my doubts.

Rafael, February 2019.

Contents

List of Figures

List of Tables

Abbreviations

AC	**A**lternating **C**urrent.
APP	**A**ctive **P**ower **P**riority.
BCSPS	**B**aja **C**alifornia **S**ur **P**ower **S**ystem.
DC	**D**irect **C**urrent.
FB	**F**ischer-**B**urmeister.
IEEE	**I**nstitute of **E**lectrical and **E**lectronics **E**ngineers.
LCCA	**L**imit **C**hecking by using **C**omplementarity condition **A**pproach.
LCSA	**L**imit **C**hecking by using **S**witching **A**pproach.
MGC	**M**exican's **G**rid *C*ode.
MPP	**M**aximun **P**ower **P**oint.
MPPT	**M**aximun **P**ower **P**oint **T**racking.
MVAR	**M**ega **V**olt **A**mpere **R**eactive.
MW	**M**ega **W**att.
NCRE	**N**on-**C**onventional **R**enewable **E**nergy
POI	**P**oint **O**f **I**nterconnection.
pu	**P**er **U**nit.
PV	**P**hotovoltaic.
RMS	**R**oot **M**ean **S**quare.
RPP	**R**eactive **P**ower **P**riority.
STC	**S**tandard **T**est **C**onditions.
VSC	**V**oltage **S**ource **C**onverter.
WLC	**W**ithout **L**imit **C**hecking.

Nomenclature

$I - V$	Current-Voltage Characteristic,
I	Current of the Photovoltaic Panel,
I_{ph}	Photocurrent of the Photovoltaic panel,
I_0	Dark saturation current of the Photovoltaic panel,
n_s	Number of Photovoltaic cells solar panel,
V_t	Diode thermal voltage,
R_s	Series resistance of Photovoltaic panel and generator,
R_{sh}	Parallel resistance of Photovoltaic panel and generator,
V_{mpp}	Maximun power point voltage,
I_{mpp}	Maximun power point current,
V_{oc}	Open circuit voltage,
I_{sc}	Short circuit current,
k	Boltzmann constant,
q	Charge of the electron,
ΔT	Temperature increment,
T	Actual module temperature,
T_n	Nominal module temperature,
ΔG	Irradiance increment,
G	Actual module irradiance,
G_n	Nominal module irradiance,
K_I	Temperature coefficient of I_{sc},
K_V	Temperature coefficient of V_{oc},
N_{ss}	Number of series connected panels,
N_{pp}	Number of parallel connected panels,

a	Diode quality ideality factor,
I_{dc}	Photovoltaic generator current,
V_{dc}	Photovoltaic generator voltage,
P_{dc}	Photovoltaic generator DC Power ,
m_a	Modulation index of VSC,
α	Firing angle of the VSC,
$G_{kk} + jB_{kk}$	Series admittance of the transformer,
$R_T + jX_T$	Series impedance of the transformer,
η	VSC's efficiency,
P_{km}	Active power flow from nodes k to m,
Q_{km}	Rective power flow from nodes k to m,
P_{mk}	Active power flow from nodes m to k,
Q_{mk}	Rective power flow from nodes m to k,
P_{nom}	Nominal active power of the VSC,
η_{inv1}	VSC's effiency at 100%,
$\eta_{inv0.5}$	VSC's effiency at 50%,
$\eta_{inv0.1}$	VSC's effiency at 10%,
pf	Power factor,
pf_{max}	Maximun power factor,
pf_{min}	Minimun power factor,
V_m	Voltage at POI,
V_k	Voltage of the VSC,
V_{ref}	Reference voltage,
K_p	Voltage droop control setting,
$P_{nom_{sv}}$	State variable for the switching approach,
$\xi_{s,c}$	State variable that module the active power of VSC,
Q_{vio}	State variable of switching approach,
Q_{max}	Maximun value of reactive power,
Q_{min}	Minimun value of reactive power,
I_{max}	Maximun current of VSC,
I_{sh}	Current of the VSC,

$\lvert S_{km}^{max} \rvert$	VSC's maximun magnitud complex power,
χ	Parameter that controls the reactive power of the VSC,
χ_s	State variable that controls the reactive power of the VSC,
χ_c	State variable that controls the reactive power of the VSC under Mexican's grid code,
χ_{max}	Maximun value of $\chi,\ \chi_s, \chi_c$,
χ_{min}	Maximun value of $\chi,\ \chi_s, \chi_c$,
P_{lim}	Active power limit,
P_{curt}	Active power curtailment,
P_{max}	Maximun active power under Mexican's grid control modes,
V_{max}	Maximun voltage under Mexican's grid control modes,
V_{min}	Minimun voltage under Mexican's grid control modes,
κ	Decision variable of Mexican's grid control modes,
$W\{\cdot\}$	Lambert function,
$\boldsymbol{\Delta P}$	Set of nodal active power mismatch equations,
$\boldsymbol{\Delta Q}$	Set of nodal active power mismatch equations,
$\boldsymbol{\Delta g}$	Set of PV Plant mismatch equations,
$\boldsymbol{\Delta h}$	Set of switching approach handling power limits mismatch equations,
$\boldsymbol{\Delta \Phi}$	Set of complementarity approach handling power limits mismatch equations,
$\boldsymbol{\Delta u}$	Set of PV Plant mismatch equations under VSC capability curve,
$\boldsymbol{x}_{nt}$	Set of nodal voltages of the network,
$\boldsymbol{x}_{pvp}$	Set of state variables for the PV Plant,
$\boldsymbol{J}$	Jacobian matrix,
TOL	Tolerance of the Newthon-Raphson method.

List of publications

Journal Papers

[1] **Tapia R.**, Fuerte-Esquivel C.R., Espinosa-Juarez E. and Sandoval T., "Steady-state model of grid-connected photovoltaic generation for power flow analysis," **IEEE Transactions on Power Systems**, ISSN: 0885-8950, Vol. 33, No. 5, September 2018, pp. 5727-5737. DOI: (10.1109/TPWRS.2018.2817585)

Conference Papers

[1] José Luis Sánchez-García; Elisa Espinosa-Juárez; **Rafael Tapia-Juárez**. Photovoltaic panel characterization by using artificial neural networks and comparison with classical models, **IEEE International Autumn Meeting on Power, Electronics and Computing (ROPEC)**, November 2015.

Chapter 1

Introduction

1.1 Research motivation

The increased integration of Photovoltaic (PV) generation plants into the electric power system is a cause of concern for the power system planners and operators because of its impact on the reliable operation of the bulk transmission system. To fully understand this impact, it is necessary to perform extensive planning and interconnection studies, which in turn requires the development of proper mathematical models of this type of generation for computer simulation studies. To achieve this objective from a steady-state operation perspective the following is necessary:

1. An approach for extracting the parameters of each PV panel making up the PV generator.
2. A mathematical representation of the solar PV plant suitable for steady-state studies that not only consider the power exchange between the PV generator and the network, but also the PV generator's dependency on environmental effects.

1.2 State of the art

1.2.1 Grid-connected photovoltaic models

In general, there is extensive work reported in the technical literature for extracting parameters of the single diode-based circuit model representing the PV panel. These parameters are obtained by iteratively solving the set of equations representing the nonlinear *I-V* characteristic of the PV panel [Xiao et al., 2006], [Chatterjee et al., 2011], [Villalva et al., 2009], [Mahmoud et al., 2012], [Soto et al., 2006], [Mahmoud and El-Saadany, 2015], based on the values of currents and voltages given in the manufacturer's datasheets under *standard test conditions* (STC) [Xiao et al., 2006], [Mahmoud et al., 2012], [Villalva et al., 2009].

On the other hand, as a first step in assessing the operation of grid-connected solar PV plants and the way in which this sort of generation affects the overall operation of an electric power system, the development of steady-state PV models suitable for power flow studies is of paramount importance. Even though the power flow study is one of the most common analyses performed in systems planning and operation [Acha et al., 2004], only a very few solar PV plant models have been proposed for power flow analysis in [Yi-Bo et al., 2008], [Ahmed and Mohsin, 2011], and [Kamh and Iravani, 2012]. In all these proposals, the large-scale PV solar park is represented by one single PV plant, which in turn is modeled as an equivalent generator. The power injected by this equivalent generator is directly included in a conventional power flow formulation, while an additional subproblem is formulated for updating the state variables of the PV plant. For this sequential solution process, the main differences between these proposals are the way in which the value of the power injected by the PV plant is determined, as well as how the PV plant state variables are maintained within limits during the computation of a feasible power flow solution.

In the mentioned coordinated sequential iterative solution process proposed in [Yi-Bo et al., 2008], the nodal voltages of the transmission network are determined by a conventional power flow analysis, and a set of nonlinear algebraic equations is then solved for the PV plant's state variables. The link between both solution processes is the electric power injected into the grid's node to which the PV plant is connected, referred to as a point of interconnection (POI), as well as the voltage magnitude and phase angle at this node. The sequential solution process is performed until all state variables of the PV plant are within limits. If one of these

state variables hits one of its limits, it is fixed at the value of the violated limit, and the power flow study is newly performed. Regarding the power flow study, the electric power injected by the PV plant, which is always working at the maximum power point (MPP), depends on the way in which the POI is categorized: PQ node or PV node. If the POI is a PQ node, the PV plant injects specified active and reactive powers. Otherwise, the PV plant only injects a specified active power, and the reactive power at the POI is determined by the power flow solution considering a controlled voltage magnitude at this node. If this reactive power violates one of its limits, it is set at this limit, and a new power flow analysis is performed by considering the POI as a PQ node.

In [Ahmed and Mohsin, 2011], the inverter's AC node is treated as an external generation node to the network, which is directly included in the conventional power flow formulation by using the nodal power equations at the inverter and POI nodes. The amount of electric power injection depends on the inverter's control mode and the type of POI at which the PV plant is embedded: PV node or PQ node. The control mode specified at the inverter's front end corresponds to a constant nodal voltage (V_{inv}-φ_{inv}) or to a constant power injection (P_{inv}^{spec}-Q_{inv}^{spec}). When the inverter is operating in a (P_{inv}^{spec}-Q_{inv}^{spec}) mode, regardless of the type of POI node, the active power P_{inv}^{spec} to be injected is given by the short circuit current of the PV array times the nominal voltage of operation, while the injected reactive power Q_{inv}^{spec} corresponds to a specified fraction of P_{inv}^{spec}. The (V_{inv}-φ_{inv}) control mode is only possible if the PV plant is connected to a PV node. In this case, the values of V_{inv} and φ_{inv} are obtained before the power flow study by performing a nonlinear analysis based on a specified transfer of active power from the inverter to the POI node. Once these values are obtained, the powers to be injected from the inverter are directly computed from the power flow equations at its front end by assuming a linear relationship between φ_{inv} and the voltage phase angle at the POI.

A generic model suitable for single-phase distributed energy resources, which includes PV plants and is intended for the analysis of distribution systems, is proposed in [Kamh and Iravani, 2012]. In this proposal, the active and reactive powers exchanged by the voltage source converter (VSC) with the grid are specified at given set points to perform a conventional power flow study. Since the VSC state variables are analytically expressed as functions of the specified injected power and the voltage magnitude at the POI, the values of these variables are computed at each iteration of the solution process to check if they are within limits. If limit violations exist, new active and reactive power set points are analytically determined

to return the VSC's state variables inside their corresponding limits before the next iteration. A similar checking of limits is performed for the voltage magnitude at the POI, but the injected power set points are heuristically calculated in case of a limit violation. This iterative process converges to a feasible power solution when none of the variables exceeds its corresponding limits.

In general terms, all the sequential methods discussed above are rather attractive because their implementation in an existing power flow, the analysis is straightforward, but caution has to be exercised because an additional set of nonlinear algebraic equations has to be solved to obtain the values of the state variables associated with each one of the single PV plants represented. Note that in this type of solution there is no way of knowing during the iterative process of the power flow solution whether or not the PV plant's state variables are within limits [Yi-Bo et al., 2008] [Ahmed and Mohsin, 2011]. If there exist limit violations of some of these variables, the power injected by the equivalent generator representing the PV solar park must be newly computed, in some cases in a heuristic way [Kamh and Iravani, 2012], to perform another power flow study. Since the sequential solution process must be performed until all state variables of the PV plant are within limits, it will not mantain a quadratic convergence.

Trying to circumvent the problems associated with the sequential approach and the concept of an equivalent generator reported in [Yi-Bo et al., 2008], [Ahmed and Mohsin, 2011] and [Kamh and Iravani, 2012], this thesis proposes the representation of the solar park by several individual PV plants tied to a collector system; each PV unit is independently modeled in the proposed power flow approach. Hence, a new power flow model for a grid-connected solar PV plant is proposed, where its state variables are simultaneously solved with those associated with the network's nodal voltages using a Newton-based unified frame of analysis. To achieve this goal, the grid-connected PV plant is considered to be composed of a set of PV panels and a DC-AC interface based on a voltage source converter (VSC), with their corresponding mathematical equations integrated in one single model. Since photovoltaic energy strongly depends on the weather conditions, both module temperature and solar irradiance are taken into account in the modeling of each PV panel. This permits considering different values of these variables for a large utility-scale solar park. Furthermore, because the VSC permits a fast and independent control of active and reactive powers at the converter's AC-side terminals, the way in which the PV plant provides a voltage control ancillary service is suitably modeled in the proposed approach. In

this context, the VSC's operative limits are considered as complementarity constraints, which are directly included in the power flow mathematical formulation using the Fischer-Burmeister (FB) merit function [Fischer, 1992], which avoids the heuristic adjustment of those limits during the iterative solution process. Lastly, the maximum power point tracking (MPPT) control strategy is also directly considered in the proposed solution approach by including the equations representing this control in the power flow formulation.

1.3 Justification

Non-Conventional Renewable Energy (NCRE) generators are now important parts of power systems. Penetration of these generators is increasing every year and it is projected that 20-30% of worldwide electricity demand would be supported by renewable generators by 2020. While this means less pollution and less dependability on fossil fuels, integration of renewable sources has its own issues, which should be taken care of. Integrating photovoltaic-based generation resources into existing power grids is challenging and requires thorough grid integration studies to assess how this kind of generation will affect the way power systems are operated and planned. Before meaningful results be obtained from those studies, realistic mathematical models for PV power plants need to be derived, coded and extensively verified in software tools used by planners and operators of electric power systems. In most instances, existing software which has been in use for many years has grown large and inflexible. Hence, modifications are achieved with great difficulty and expense. This has provided the motivation for developing afresh, well-designed and efficient software where both well established electric components as well as PV power plants can be modelled along side each other with a minimum effort.

Arguably, power flow (load flow) analysis is the most popular power systems computer calculation performed in systems planning and operation. Bearing this in mind and as a starting point, the efforts in this research are concentrated on tackling the steady-state, positive sequence modelling and analysis of PV power plants. Furthermore, the power flow algorithm has been selected to verify the proposed PV power plant model considering the following:

i) A PV plant model for power flow studies that depends on wheather conditions and can operate under different control modes.

ii) The PV plant model considerers operational limits in the converter as well as take into account the capability curve.

iii) The PV plant model includes control modes that meet with the Mexican's grid code.

1.4 Research Objectives

The general objectives of this research are summarized as follows:

i) To develop a comprehensive and general approach in a unified single frame of reference for the analysis of power flows in electric power systems containing grid-connected PV plants.

ii) To develop a model for the PV plant that complies with the requirements of interconnection described in the Mexican's grid code in the context of power flow studies.

iii) To develop a general PV plant model that permits representation of a PV power plant by a single machine equivalent model or by multiple machine models, including the operative limits of the converter.

iv) To develop a highly efficient method which combines simultaneously the state variables corresponding to the PV plant with the nodal voltage magnitudes and angles of the network in a single frame-of-reference for a unified, iterative solution through a Newton-Rapshon technique.

1.5 Methodology

The proposed methology that has been adopted in order to achieve the previous objectives is described as:

i) A full review of previous works in the area of PV panel models as well as the techniques used for parameters' estimation of a single diode photovoltaic model. A survey is also made for current steady state PV plant models, suitable for power flow studies taking into account plant operating limits. To develop a practical methology that permits the extraction parameters of PV panel.

ii) To develop a set of nonlinear equations that represent the interaction between a PV generator and a VSC, considering the control modes of operation for the converter and their operative limits using complementarity constraints.

iii) To include the set of equations associated to the PV plant together with the VSC's operative limits into the Newton power flow formulation in a unified frame of analysis. Suitable initialization of the state variables for reliable iterative solutions is duty addressed.

iv) To develop a digital algorithm that solves the conventional power flow analysis including PV plant models in a unified way.

v) To test the proposed approach considering a modified IEEE 14-bus test system and an equivalent 71-bus from a real power system.

1.6 Contributions

The main contributions of the proposed approach are the following:

i) A new and comprehensive model for a PV plant is developed starting from basic PV arrangement considering different control modes of operation.

ii) A PV solar park is assumed to be composed of several PV plants, which allows considering different collection grid topologies.

iii) The power flow approach simultaneously combines the state variables corresponding to the PV plants composing the PV solar park with the nodal voltage magnitudes and angles of the network in a single frame of reference. The result is a unified, iterative solution that retains Newton's quadratic convergence characteristics.

iv) Operative limits of PV plants' state variables are checked within iterations and adjusted during the power flow solution process using complementarity constraints. There is no need to have a special part of the code or to solve another subproblem to check the limits.

v) The power flow problem is formulated in a very flexible way, considering PV power parks composed of multiples PV plants operating with differents control modes, operational limits, capabilities and control strategies.

vi) Finally, the power flow solution obtained by the proposed approach is applied to acomplish with the requirements of interconnection described in the Mexican's grid code.

1.7 Thesis outline

The remainder of this thesis is organized as follows.

Chapter 2 presents the mathematical formulation of the single diode-based PV panel as well as the voltage source converter VSC. The resulting set of nonlinear equations is assembled together with the power network's equations to formulate a generalized power flow problem in a unified frame of reference. In this context, it is reported the way in which all operation and control mode constraints of the PV plant are considered in the power flow formulation.

Chapter 3 illustrates the applicability of the newly developed models for the analysis within conventional power flows. Furthermore, discussions and comparisons based on results obtained from the implementation and application of the proposed approach are presented, demonstrating its feasibility and benefits.

Chapter 4 gives the general conclusions of this thesis and presents suggestions for future research.

Chapter 2

Steady-State Modeling of a Power System with Embedded Photovoltaic Generation

2.1 Introduction

In this chapter, models of a single diode-based PV panel and a voltage source converter are derived from basic principles. These are formulated in such a way that they are put together in a single PV power plant model that can be used within power flow-like formulations, for efficient solutions. A detailed description of the control operating modes associated with voltage source converters is also provided, together with the way in which these control modes are included in the power flow formulation. A general strategy for selecting initialvalues for the state variables of PV plants is also presented.

2.2 Mathematical formulation

2.2.1 Photovoltaic Panel model

As in several system simulation platforms [Villalva et al., 2009],[Chatterjee et al., 2011], the single diode model shown in Fig. 2.1 is used to describe the equivalent circuit of a PV panel composed of a set of n_s PV cells connected in series. The

PV panel has an equivalent I-V characteristic given by [Villalva et al., 2009]:

$$I = I_{ph} - I_0 \left[\exp\left(\frac{V + IR_s}{V_t} \right) - 1 \right] - \frac{V + IR_s}{R_{sh}}, \tag{2.1}$$

where V_t, I_{ph}, I_0, R_s and R_{sh} are unknown parameters defined as follows: V_t is the diode thermal voltage, I_{ph} is the photocurrent and I_0 is the dark saturation current. On the other hand, R_s and R_{sh} are the series and parallel resistances, respectively.

The first three parameters V_t, I_{ph} and I_0 are estimated as reported in [Villalva et al., 2009] based on the values of V and I at the terminals of the PV panel. For this purpose, the values of (V, I) are taken from the manufacturer's datasheets at STC (25°C and 1000W/m^2) for the following operating modes: short circuit $(0, I_{sc})$, MPP (V_{mpp}, I_{mpp}), and open circuit $(V_{oc}, 0)$. Hence, the diode thermal voltage is given by [Villalva et al., 2009],[Chatterjee et al., 2011]:

$$V_t = n_s \frac{kTa}{q}, \tag{2.2}$$

where k is the Boltzmann constant $(1.38 \times 10^{-23} J/K)$, T is the actual module temperature in K, a is the diode ideality factor and q is the electron charge $(1.6021 \times 10^{-19} C)$.

The photocurrent I_{ph} is given by (2.3) as a function of the irradiance and temperature

$$I_{ph} = (I_{sc} + K_I \Delta_T) \frac{G}{G_n}, \tag{2.3}$$

where $\Delta_T = T - T_n$, T_n is the nominal module temperature in K, G and G_n are the actual and nominal irradiance in W/m^2 and K_I is the temperature coefficient of I_{sc}. Finally, I_0 is expressed by

$$I_0 = \frac{I_{sc} + K_I \Delta_T}{\exp\left((V_{oc} + K_V \Delta_T) / V_t \right) - 1}, \tag{2.4}$$

where V_{oc} is the open circuit voltage and K_V its temperature coefficient.

On the other hand, if (2.1) is applied at the MPP, the relationship (2.5) is derived by considering the concept of DC power $P = IV$. Hence, the unknown values of

R_s and R_{sh} can be obtained by iteratively solving (2.1) and (2.5):

$$\frac{\partial P}{\partial V} = \frac{\partial I}{\partial V} V + I = 0. \tag{2.5}$$

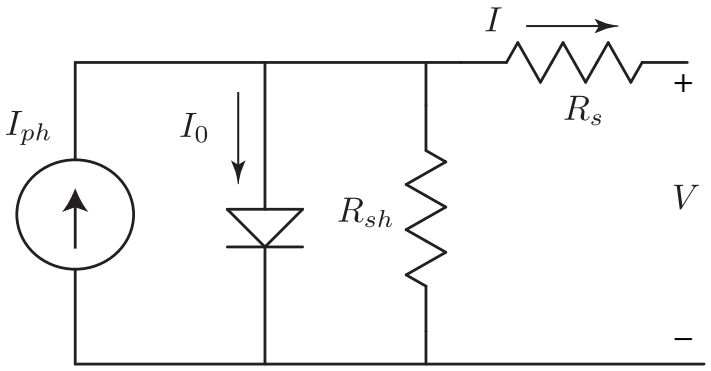

FIGURE 2.1: PV panel electrical equivalent circuit.

2.2.2 PV generator model

A PV generator is made up by an array of series and parallel-connected PV panels that have the same manufacturing characteristics. Based on the structure shown in Fig. 2.2, the equivalent circuit representing the PV generator is then defined by the parameters given by [Chatterjee et al., 2011]:

$$I_{eq} = I_{eq} \times N_{pp} \qquad \forall\ eq = sc, ph, 0, dc \tag{2.6}$$

$$V_{eq} = V_{eq} \times N_{ss} \qquad \forall\ eq = oc, t, dc \tag{2.7}$$

$$R_{eq} = R_{eq} \times N_{ss}/N_{pp} \qquad \forall\ eq = s, sh, \tag{2.8}$$

where N_{ss} and N_{pp} are the number of panels connected in series and parallel, respectively, and I_{dc} and V_{dc} are the current and voltage of the PV generator at its DC terminals. Note also that the diode ideality factor a keeps the same value for the PV generator model [Chatterjee et al., 2011].

2.2.3 Grid-connected PV plant model

The PV generator delivers DC power that is injected into the grid as an AC power through a point-to-point VSC-based DC-AC link, as shown in Fig. 2.2. In this case, the VSC is operating under a MPPT control mode to maximize the amount of

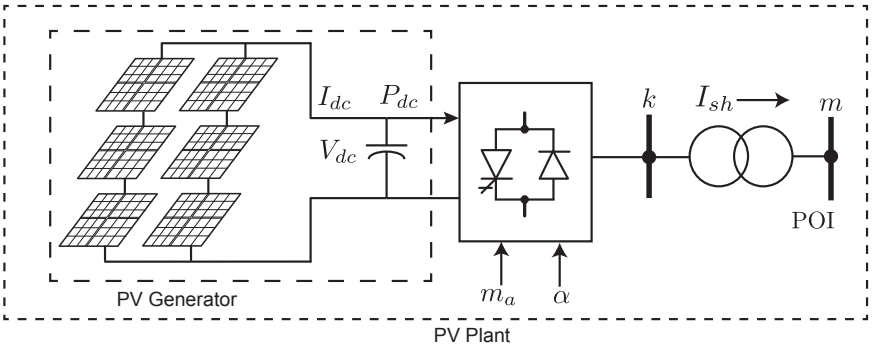

FIGURE 2.2: PV plant system.

power converted from the PV generator. According to [Ahmed and Mohsin, 2011], the line-to-line three-phase RMS voltage at bus k is expressed by (2.9), where m_a and α are the modulation index and firing angle of the VSC, respectively:

$$\overline{\mathbf{V_k}} = \sqrt{3/8} m_a V_{dc} \angle \alpha. \tag{2.9}$$

The model also includes a transformer with a series admittance given by $G_{kk} + jB_{kk} = 1/(R_T + jX_T)$, which provides a Galvanic insulation [Milano, 2010]. Based on this admittance and (2.9), the active and reactive powers that flow from k to m are given by

$$\begin{aligned} P_{km} &= \frac{3}{8} m_a^2 V_{dc}^2 G_{kk} + \sqrt{3/8} m_a V_{dc} V_m \\ &\quad \times \left[G_{km} \cos(\alpha - \theta_m) + B_{km} \sin(\alpha - \theta_m) \right] \qquad (2.10) \\ Q_{km} &= -\frac{3}{8} m_a^2 V_{dc}^2 B_{kk} + \sqrt{3/8} m_a V_{dc} V_m \\ &\quad \times \left[G_{km} \sin(\alpha - \theta_m) - B_{km} \cos(\alpha - \theta_m) \right]. \qquad (2.11) \end{aligned}$$

2.2.4 VSC's power balance equation

The power balance equation through the VSC can be expressed as a function of the power converter's efficiency η, $\eta = P_{km}/P_{dc}$ [Rampinelli et al., 2014], and it is given by

$$P_{km} = \eta P_{dc} = \eta V_{dc} I_{dc}. \tag{2.12}$$

The efficiency depends on the inverter power output and remains almost constant for values of output powers above 0.3 p.u. [Monteiro et al., 2016] such that the efficiency can be set to a fixed value. On the other hand, an explicit relationship

between the efficiency and the converter's output power is given by the Jantsch's model [Monteiro et al., 2016]:

$$\eta = \frac{\frac{P_{km}}{P_{nom}}}{\frac{P_{km}}{P_{nom}} + k_0 + k_1\frac{P_{km}}{P_{nom}} + k_2(\frac{P_{km}}{P_{nom}})^2}, \tag{2.13}$$

where P_{nom} is the converter's nominal power. The parameters k_0, k_1 and k_2 are computed by (2.14)-(2.16) as functions of the converter's efficiency at 100, 50 and 10% of its rated output power: η_{inv1}, $\eta_{inv0.5}$ and $\eta_{inv0.1}$ [Monteiro et al., 2016].

$$k_0 = \frac{1}{9}\frac{1}{\eta_{inv1}} - \frac{1}{4}\frac{1}{\eta_{inv0.5}} + \frac{5}{36}\frac{1}{\eta_{inv0.1}} \tag{2.14}$$

$$k_1 = -\frac{4}{3}\frac{1}{\eta_{inv1}} + \frac{33}{12}\frac{1}{\eta_{inv0.5}} - \frac{5}{12}\frac{1}{\eta_{inv0.1}} - 1 \tag{2.15}$$

$$k_2 = \frac{20}{9}\frac{1}{\eta_{inv1}} - \frac{5}{2}\frac{1}{\eta_{inv0.5}} + \frac{5}{18}\frac{1}{\eta_{inv0.1}}. \tag{2.16}$$

Lastly, the efficiency curve with values of $\eta_{inv1} = 0.98, \eta_{inv0.5} = 0.98, \eta_{inv0.1}0.96$ is shown in Fig. 2.3 [Monteiro et al., 2016].

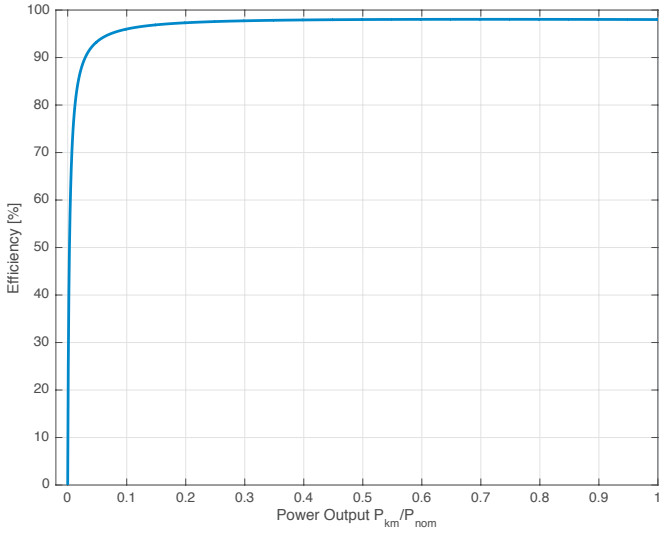

FIGURE 2.3: Efficiency curve.

2.2.5 Basic mismatch equations of the PV plant

The general set of mismatch equations that describes the steady-state operation of the PV power plant always considers the basic equations (2.17) and (2.19). The

MPPT control strategy is represented by (2.17)-(2.18), which are derived from (2.1) and (2.5), respectively. The active power flow mismatch equation at the AC terminals of the VSC is given by (2.19):

$$\begin{aligned}\Delta g_1 &= I_{ph} - I_0\left[\exp\left(\frac{V_{dc}+I_{dc}R_s}{V_t}\right)-1\right] \\ &\quad - \frac{V_{dc}+I_{dc}R_s}{R_{sh}} - I_{dc} = 0 \qquad (2.17)\\ \Delta g_2 &= I_{dc} - V_{dc}\left[\frac{I_0}{V_t}\exp\left(\frac{V_{dc}+I_{dc}R_s}{V_t}\right)+\frac{1}{R_{sh}}\right] / \\ &\quad \left[\frac{I_0 R_s}{V_t}\exp\left(\frac{V_{dc}+I_{dc}R_s}{V_t}\right)+\frac{R_s}{R_{sh}}+1\right] = 0 \qquad (2.18)\\ \Delta g_3 &= \eta P_{dc} - P_{km} = 0. \qquad (2.19)\end{aligned}$$

On the other hand, the reactive power flow mismatch equation to be considered depends on the control mode at which the VSC is operating, as described in the next subsection.

2.2.6 VSC's control modes

Since the grid-connected PV plant can provide ancillary services associated with the voltage magnitude control, the following control modes have been considered for the VSC.

2.2.6.1 PQ control mode

In this control mode the VSC injects an active power P_{km} according to the network operation conditions and also provides reactive power support. This power support depends on the converter's power factor (pf) and the injected active power P_{km}:

$$\Delta g_4 = Q_{km} - P_{km}\tan\left(\cos^{-1}(pf)\right) = 0, \qquad (2.20)$$

where pf is a fixed value selected within the range of $pf_{min} \leq pf_{lag} \leq pf_{max}$ or $-pf_{min} \leq pf_{lead} \leq -pf_{max}$. The steady-state operation of the PV plant for this control mode is then obtained by solving the mismatch equations (2.17)-(2.20) for the four state variables V_{dc},I_{dc},m_a and α.

2.2.6.2 PV control mode

This kind of control mode permits the participation of PV units in ancillary services, such as reactive power support and voltage control. This is a requirement in the Mexican grid code for the integration of PV plants at the transmission level [Comisión Reguladora de Energía, 2006]. In this control mode, an active power P_{km} is injected into the network, and the voltage magnitude V_m at the POI is controlled at a constant value V_{ref} by the VSC. This control is achieved by adjusting the VSC's reactive power during the iterative solution process based on the voltage droop control given by [REMTF, 2010]:

$$\Delta g_5 = V_m - V_{ref} + K_p Q_{km} = 0, \tag{2.21}$$

where K_p represents the voltage droop control setting. Note that (2.21) is used for each PV plant that provides reactive power support to achieve the voltage magnitude control at the m-th bus [De Brabandere et al., 2007],[Elrayyah et al., 2014].

The nonlinear equations that need to be solved to assess the steady-state operation under this control mode are (2.17), (2.18), (2.19) and (2.21). Note that in this case the VSC applies both MPPT and voltage droop control strategies to achieve maximum power and voltage control.

Note also that the final value of α is relative to the system phase reference, regardless if the VSC is operating under a PQ or PV control mode.

2.3 Handling of the VSC power limits

The handling of VSC's power limits is performed by considering either of the following two approaches: i) a switching approach, which is applied at the end of each iteration of the solution process, or ii) a complementarity constraints approach, where mismatch constraints of power limits are directly introduced in the power flow formulation. In both cases, the dimension of the problem formulation remains unaltered during the solution process, and V_{dc}, I_{dc}, m_a and α prevail as state variables of the PV plant along with additional state variables added by the selected limit checking approach.

2.3.1 Switching approach

Our proposal in this approach is to extend the set of equations representing the PV plant with mismatch equations associated with the limit violation of active and reactive powers. The number of mismatch equations is one (resp. two) for the PQ (resp. PV) control mode of operation. Furthermore, one (resp. two) additional state variable is (resp. state variables are) added to avoid oversizing the total number of nonlinear equations associated with the power flow formulation. The limit checking is performed at the end of each iteration once the maximum absolute value of the mismatch equations is lower than 1×10^{-3}.

2.3.1.1 Active power limits

In both control modes, the VSC is operating within limits if $\eta V_{dc} I_{dc} \leq P_{nom}$. Hence, (2.22) must be added to the set of equations representing the steady-state operation of the PV plant, and $P_{nom_{sv}}$ is an extra state variable of the problem. In addition, for both operating control modes (2.18) is rewritten as (2.23), where ξ_s will have a non-null value if there exists a limit violation. While the VSC is operating within limits, $P_{nom_{sv}}$ is a state variable, and ξ_s is maintained at its null initial value. If the limit violation takes place, $P_{nom_{sv}}$ is fixed at P_{nom}, and ξ_s replaces $P_{nom_{sv}}$ as a state variable. Note that in this case the values of V_{dc} and I_{dc} must satisfy $\eta V_{dc} I_{dc} = P_{nom}$, which implies that the VSC is not longer operating under MPP mode:

$$\Delta h_1 = P_{nom_{sv}} - \eta V_{dc} I_{dc} = 0, \tag{2.22}$$

$$\Delta h_2 = \Delta g_2 + \xi_s = 0. \tag{2.23}$$

2.3.1.2 Reactive power limits

The amount of reactive power provided by the VSC depends on the values of P_{km}, which change during the iterative solution process, and the value of pf. For the PQ control mode of operation, the value of pf is specified by the user, which must be selected within the ranges defined in Section 2.2.6.1; if this value is selected out of limits, however, the pf is automatically fixed at the value of the limit. For the PV control mode, the limit value of reactive power that the VSC can either absorb or inject to satisfy $Q_{min} \leq Q_{km} \leq Q_{max}$ is given by (2.24) or (2.25), respectively. Hence, the limits handling is performed by adding

(2.26) to the set equations representing the PV plants steady-state operation. The voltage magnitude control is achieved while Q_{km} is within limits such that Q_{vio} is considered as a state variable. Note that if there is no limit violation, $Q_{vio} = Q_{km}$ at the end of the solution process. Otherwise, Q_{vio} is fixed at the violated limit, and V_{ref} becomes the new state variable such that the voltage magnitude at the POI is not longer controlled:

$$Q_{min} = P_{km} \tan\left(\cos^{-1}\left(-pf_{min}\right)\right) \quad (2.24)$$

$$Q_{max} = P_{km} \tan\left(\cos^{-1}\left(pf_{min}\right)\right) \quad (2.25)$$

$$\Delta h_3 = Q_{vio} - Q_{km} = 0. \quad (2.26)$$

2.3.2 Complementarity conditions approach

In general, a complementarity condition is expressed as $y_{min} \leq y \leq y_{max} \perp C_L(y) = 0$ [Rosehart et al., 2006] and states an equilibrium between the control law $C_L(y)$ of the VSC and the rating limits y_{min} and y_{max} of its variable y. This complementarity condition is transformed into the set of nonlinear equality constraints given by (2.27)-(2.29), which is directly included in the power flow formulation. In this case, z_a and z_b are a new pair of state variables of the problem that relaxes (2.27), which avoids the resultant set of equations associated with the VSC operation being oversized. Note that (2.27) is not considered in the formulation if there is not a control law equation:

$$C_L(y) - z_a + z_b = 0 \quad (2.27)$$

$$\sqrt{(y - y_{min})^2 + z_a^2} - \left[(y - y_{min}) + z_a\right] = 0 \quad (2.28)$$

$$\sqrt{(y_{max} - y)^2 + z_b^2} - \left[(y_{max} - y) + z_b\right] = 0. \quad (2.29)$$

On the other hand, (2.28) and (2.29) represent the FB merit function [Fischer, 1992], which can be improved with the following function:

$$\sqrt{\left[(y - y_{min}) - z_a\right]^2 + 4\mu^2} - \left[(y - y_{min}) - z_a\right] = 0 \quad (2.30)$$

$$\sqrt{\left[(y_{max} - y) - z_b\right]^2 + 4\mu^2} - \left[(y_{max} - y) - z_b\right] = 0 \quad (2.31)$$

presented in [Facchinei et al., 1999]. This function is smooth (continuously differentiable) for every $\mu = 0$.

2.3.2.1 Active power limits

The set of nonlinear equations used to satisfy $\eta V_{dc} I_{dc} \leq P_{nom}$ is (2.32), which was rewritten from (2.18), and (2.33) for both control modes of operation. When the PV generator oversteps its limit, the state variable ξ_c takes a value different from zero, steering the VSC operation point out of the MPP:

$$\Delta\Phi_1 = \Delta g_2 + \xi_c = 0 \tag{2.32}$$

$$\Delta\Phi_2 = \sqrt{\xi_c^2 + (P_{nom} - \eta V_{dc} I_{dc})^2} - [\xi_c + (P_{nom} - \eta V_{dc} I_{dc})] = 0. \tag{2.33}$$

2.3.2.2 Reactive power limits

When the VSC is operating in the PQ control mode, the reactive power limits are handled as explained for the switching approach. On the other hand, the set of equations (2.34)-(2.36) is used in the PV control mode to assure that $Q_{min} \leq Q_{km} \leq Q_{max}$ when a voltage magnitude control is performed based on the voltage droop control strategy. Note that in this approach (2.21) is rewritten as (2.34):

$$\Delta\Phi_3 = \Delta g_5 - v_a + v_b = 0 \tag{2.34}$$

$$\Delta\Phi_4 = \sqrt{(Q_{km} - Q_{min})^2 + v_a^2} - \big[(Q_{km} - Q_{min}) + v_a\big] = 0 \tag{2.35}$$

$$\Delta\Phi_5 = \sqrt{(Q_{max} - Q_{km})^2 + v_b^2} - \big[(Q_{max} - Q_{km}) + v_b\big] = 0. \tag{2.36}$$

2.4 VSC's Capability

The maximum amount of active and reactive power that the VSC can inject into the system is limited by its maximum current capacity. Hence, the VSC's magnitud of complex power is given in terms of its AC voltage V_k and the maximun current I_{max} [Stijn, 2010] by

$$|S_{km}^{max}| = |V_k||I_{max}| = \sqrt{P_{km}^2 + Q_{km}^2} \tag{2.37}$$

where $|S_{km}^{max}|$ is the VSC's maximun magnitud of complex power. The inverter operating space in the PQ plane is given by the semicircle

$$(P, Q) : 0 \leq P_{km} \leq P_{lim}, \left| Q_{km} \leq \sqrt{(V_k I_{max})^2 - P_{km}^2} \right| \tag{2.38}$$

shown in Fig. 2.4. Note that PQ plane contour is given by $P_{lim} = V_k I_{max} = S_{km}^{max}$. Furthermore, the VSC's current I_{sh} should be within the inverter's thermal capability: $I_{sh} \leq I_{max}$ [Zhang, 2004].

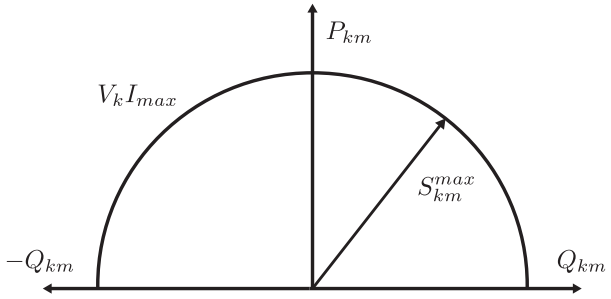

FIGURE 2.4: VSC's capability curve.

2.4.1 Basic mismatch equations of the PV plant using VSC's capability

Based on what was mentioned in the last section, a new formulation approach is the VSC operating in the PQ plane space in terms of the maximum current capability. Hence, and similar to section 2.2.5, the set of basic equations representing a PV plants is described as:

$$\begin{aligned}
\Delta u_1 &= I_{ph} - I_0 \left[\exp\left(\frac{V_{dc} + I_{dc}R_s}{V_t}\right) - 1\right] \\
&\quad - \frac{V_{dc} + I_{dc}R_s}{R_{sh}} - I_{dc} = 0 \qquad (2.39) \\
\Delta u_2 &= I_{dc} + \xi_s - V_{dc}\left[\frac{I_0}{V_t}\exp\left(\frac{V_{dc} + I_{dc}R_s}{V_t}\right) + \frac{1}{R_{sh}}\right] / \\
&\quad \left[\frac{I_0 R_s}{V_t}\exp\left(\frac{V_{dc} + I_{dc}R_s}{V_t}\right) + \frac{R_s}{R_{sh}} + 1\right] = 0 \qquad (2.40) \\
\Delta u_3 &= \eta P_{dc} - P_{km} = 0 \qquad (2.41) \\
\Delta u_4 &= I_{sh} - \frac{\sqrt{V_k^2 + V_m^2 - 2V_k V_m \cos(\alpha - \theta_m)}}{\sqrt{R_T^2 + X_T^2}} = 0 \qquad (2.42) \\
\Delta u_5 &= \sqrt{\xi_s^2 + (P_{lim} - P_{km})^2} - [\xi_s + (P_{lim} - P_{km})] = 0. \qquad (2.43)
\end{aligned}$$

Note that the new equation (2.42) corresponds to the current I_{sh} through the VSC, as shown in Fig. 2.2. Since the active and the reactive power limits are handled by using the complementarity approach, (2.39)-(2.43) are the set of mismatch equations asociated with the state variables $I_{dc}, V_{dc}, \alpha, I_{sh}$ and ξ_s. Finally, the values of state variables m_a and P_{lim} will depend not only of the control strategy

but also the control mode at which the VSC is operating. The same line of reasoning applies to the way in which the inverter reactive power flow mismatch equation is formulated and to the inverter reactive power limits.

2.5 PV-VSC Control strategy, control operating modes and handling of power limits

The specified control strategies for the PV-VSC power plant are divided into two main groups, Active Power Priority (APP) and Reactive Power Priority (RPP). On the other hand, the specified VSC's control modes associated with each control strategy depend on how the reactive power is dispatched, while the power limits ensure the safe operation of the converter.

2.5.1 Active Power Priority

In this control strategy the amount of reactive power injected into the grid depends of the active power available. The reactive power is limited by $V_k I_{max}$ and P_{km} at that moment. The control modes associated to this strategy are described below.

2.5.1.1 *APP* PQ control mode

In this control mode the VSC injects an active power P_{km} according to the weather conditions of the PV Generator and to the system's operating conditions, as given by (2.10). For a given active power output P_{km1}, the set of reactive powers that can be injected or absorbed by the VSC is given by the vertical segment shown in Fig. 2.5 a). Note also that the reactive power capability in this segment is limited by the inverter rating $|S_{km}^{max}| = |V_k||I_{max}|$, which will change according to the active power output. In this context, the entire inverter rating can be utilized to supply or absorb reactive power when no active power is produced.

Based on the mentioned above, the reactive power support defined by the line segment is mathematically represented by

$$\Delta g_6 = Q_{km} - \chi\sqrt{(V_k I_{max})^2 - P_{km}^2} = 0 \tag{2.44}$$

where the parameter χ can take a fixed value within the range given by $-1 \leq \chi \leq 1$. Furthermore, the constraint $P_{lim} = V_k I_{max}$ ensures that the VSC will not be overload by its maximun current, while m_a is the state variable associated to (2.44). Lastly, the physical interpretation of this combination of control strategy and control mode is that the reactive power to be injected or absorbed by the VSC is a fixed weighted value χ times the root square of the difference of the squares of the apparent power and active power of the VSC.

2.5.1.2 *APP* PQ control mode-fixed power factor

In this case, the PV inverter is required to operate at a fixed value of power factor pf. Hence, for a given active power output P_{km}, the reactive power Q_{km} must be adjusted along the corresponding line segment to achieve the specified pf. In order to achieve that adjustment, the weighting factor χ is now a state variable χ_s. The geometric representation of this control mode is schematically shown in Fig. 2.5 b). On the other hand, the combination of these control strategy and control mode is mathematically represented by the following set of equations,

$$\Delta u_7 = Q_{mk} - P_{mk}\tan(\text{acos}(pf)) - \rho_a + \rho_b = 0 \quad (2.45)$$

$$\Delta u_8 = Q_{km} - \chi_s\sqrt{(V_k I_{max})^2 - P_{km}^2} = 0 \quad (2.46)$$

$$\Delta u_9 = \sqrt{\left[(\chi_s - \chi_{min}) - \rho_a\right]^2 + 4\mu^2} - \left[(\chi_s - \chi_{min}) - \rho_a\right] = 0 \quad (2.47)$$

$$\Delta u_{10} = \sqrt{\left[(\chi_{max} - \chi_s) - \rho_b\right]^2 + 4\mu^2} - \left[(\chi_{max} - \chi_s) - \rho_b\right] = 0 \quad (2.48)$$

In this case, the state variable associated with (2.45) is m_a. On the other hand, the state variable χ_s represents the reactive power adjustment during the solution process to achieve an inverter operation at the required pf. This state variable is limited by the complementarity constraints (2.47) and (2.48) at the limitis $-1 \leq \chi_s \leq 1$. In this context, Fig 2.5 b) clearly shows that for a value of P_{km_1} the maximum pf is obtained when the state variable χ_s equals 1: its maximum value. On the other hand, if for the same value of active power the inverter pf_1 is reduced to a value of pf_2, the state variable χ_s must be adjusted to a value of 0.5. Note also that the inverter operates in a unitary pf for a value of P_{km_2}, which means that no reactive power is provided by the inverter and χ_s is null. Lastly, the active power limit is given by $P_{lim} = V_k I_{max}$.

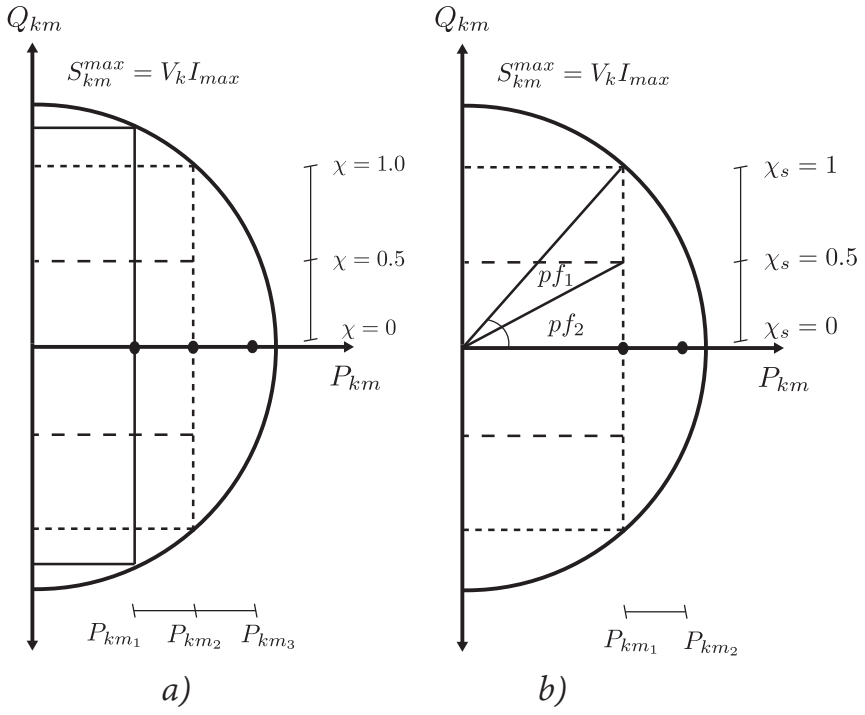

FIGURE 2.5: Active Power Priority. Geometric representation of control modes *PQ* and *PQ (pf)*

2.5.1.3 *APP* PV control mode

This kind of control mode represents the participation of PV plant units in ancillary services such as the control of voltage magnitude. In this control mode, an active power P_{km} is injected into the network, and the voltage magnitude V_m at the POI is controlled at a constant value V_{ref} by the VSC. This control is mathematically formulated by the following set of equations,

$$\Delta u_{11} = V_m - V_{ref} + K_p Q_{km} = 0 \tag{2.49}$$

$$\Delta u_{12} = \sqrt{\left[(Q_{km} - Q_{min}) - v_a\right]^2 + 4\mu^2} - \left[(Q_{km} - Q_{min}) - v_a\right] = 0 \tag{2.50}$$

$$\Delta u_{13} = \sqrt{\left[(Q_{max} - Q_{km}) - v_b\right]^2 + 4\mu^2} - \left[(Q_{max} - Q_{km}) - v_b\right] = 0 \tag{2.51}$$

For this control mode m_a is the state variable associated with (2.49). Furthermore, the reactive power that the VSC can either absorb or inject is constrained to $Q_{min} \leq Q_{km} \leq Q_{max}$. These limits are given by $Q_{min} = -\sqrt{(V_k I_{max})^2 - P_{km}^2}$ and $Q_{max} = \sqrt{(V_k I_{max})^2 - P_{km}^2}$ and ensure to not overload the VSC. This behavior is represented by the constraints (2.50) and (2.51). On the other hand, $P_{lim} = V_k I_{max}$.

2.5.2 Reactive Power Priority

For this control strategy, the production of reactive power is prioritized over the production of active power, which implies a curtailment of active power if there is not sufficient capacity in the VSC to inject the required reactive power [Ding et al., 2016]. For this control strategy the following two control modes are proposed.

2.5.2.1 *RPP* PQ control mode

The aim of the present control mode is to inject a fixed amount of reactive power that is defined as a fixed percentage χ of S_{km}^{max}:

$$\Delta u_{14} = Q_{km} - \chi V_k I_{max} \tag{2.52}$$

If for a given active power output P_{km} there is not enough room of reactive power capability to acomplish that requirement, the active power P_{km} is curtailed to a value P_{curt} given by $P_{lim} = P_{curt} = V_k I_{max}\sqrt{1-\chi}$. In this case, the parameter χ can take a value within [-1,1] and m_a is the state variable associated with (2.52).

2.5.2.2 *RPP* PV control mode

In this control mode, and similarly to Section 2.5.1.3, the voltage magnitude is controlled at the POI based on the control law (2.49) but instead of constraining the active and reactive power through equations (2.43) as well as (2.50) and (2.51) these powers are constrained based on the parameter χ as follows:

$$P_{lim} = P_{curt} = V_k I_{max}\sqrt{1-\chi} \tag{2.53}$$

$$Q_{min} = -\chi V_k I_{max} \tag{2.54}$$

$$Q_{max} = \chi V_k I_{max} \tag{2.55}$$

Fig. 2.6 shows the law control of the VSC to curtail the active power P_{km} into P_{curt}. When the output of active power is P_{km_1} there is not enough reactive power Q_{km_1} to accomplish with χS_{km}^{max}. Hence P_{km_1} has to be curtailed to a value of P_{curt} where $Q_{km_2} > Q_{km_1}$. This curtailment means that the PV plant is not operating at the MMP anymore because the VSC steers the MPP at P_{dc_1} toward a new operating point at lower DC Power P_{dc_2}. Note that this new operating

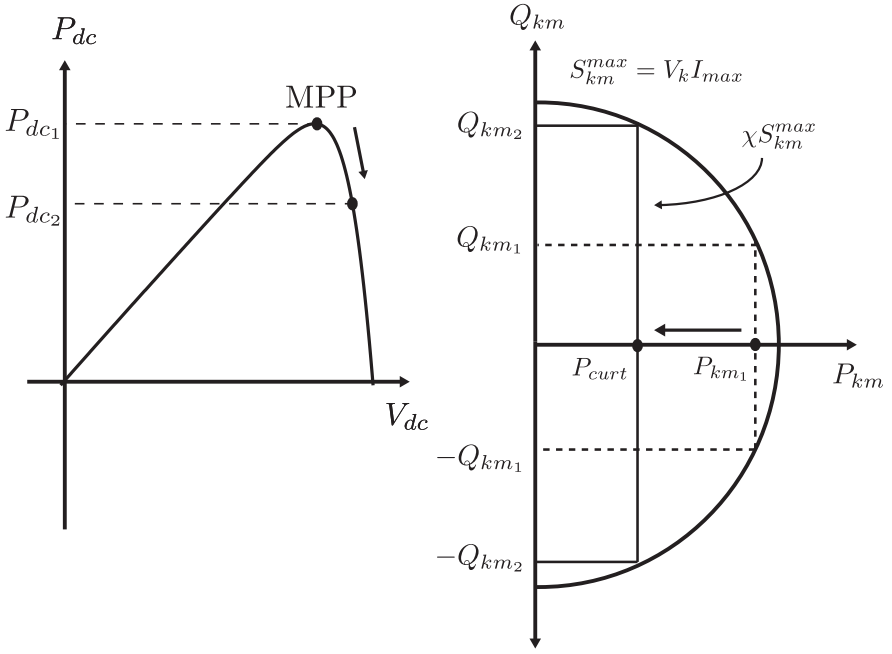

FIGURE 2.6: Rective Power Priority. Geometric representation of control modes PQ and PV

point corresponds to the AC output power P_{curt}. This reduction of active power is performed only for Reactive Power Priority strategy through (2.40) and (2.43).

2.6 Mexican's Grid Code

The Mexican Grid code [Comisión Reguladora de Energía, 2016] establishes the requeriments to provide ancillary services by grid-connected asynchronous resources, like PV plants and wind-based generators. These requirements are classified according to maximun active power capacity of the generator to be interconnected to the Mexican national electrical system. In this context, Figs. 2.7 and 2.8 show the reactive power requirements as well as the voltage magnitude for the interconnection of asynchronous resources type C and D, respectively.

The reactive power requeriments for Fig. 2.7 depends on the level of active power P_{mk} and the value of P_{max}. In this context, two zones in the ordinate axis are identified as Upper and Lower Zone, respectively. When the asynchronous resources operates at Upper Zone, the active power P_{mk} must be kept within the range of $0.5P_{max} \leq P_{mk} \leq P_{max}$. On the other hand, the maximun reactive power that

can be injected into the grid is a function of P_{mk} and is given by $Q_{mk} = 0.33P_{mk}$, which implies a maximun leading and lagging power factor of $pf = \pm 0.9496$. Regarding the operation in the Lower Zone, the value of P_{mk} varies within the range of $0 < P_{mk} < 0.5P_{max}$, while the maximun value of Q_{mk} corresponds to $\frac{0.33}{0.5}\frac{P_{mk}^2}{P_{max}}$. Note that when the P_{mk} tends to 0, the pf tends to 1. Fig. 2.8 is the projection of Fig. 2.7 with the voltage magnitude V_m in the z axis. In this sense, the requirements explained above must be taken into account to maintain the voltage magnitude within limits given by $0.95 \leq V_m \leq 1.05$. In order to accomplish the reactive and voltage requirements of the Mexican's grid code shown in these Figs., three different control modes are proposed and derived from basic principles in the following subsections.

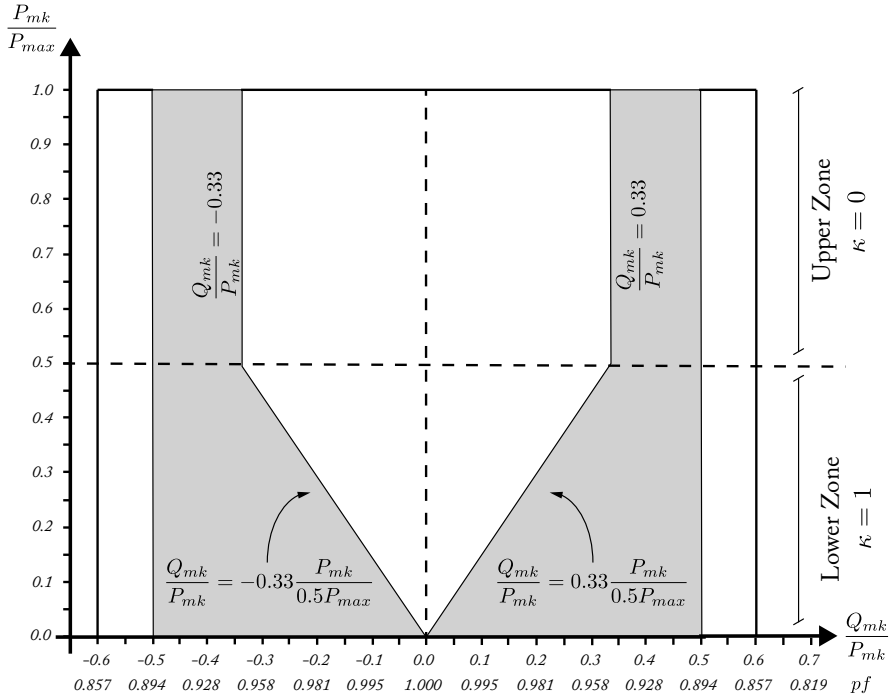

FIGURE 2.7: Diagram $\frac{Q_{mk}}{P_{mk}}, \frac{P_{mk}}{P_{max}}$ for asynchronous resources.

2.6.1 VSC Mexican's Grid Code control modes

In order to accomplish the requeriments of the Mexican's Grid Code (MGC), three main consideration need to be taken into account based on Fig 2.8, and the VSC's operating capability (2.37): i) it is necessary a curtailment of active power (P_{max}) to meet the reactive power reserve, ii) the reactive power injected into the grid depends on the VSC's active power output. In this case, the boundary between two different regions of reactive power operation is defined by an active power

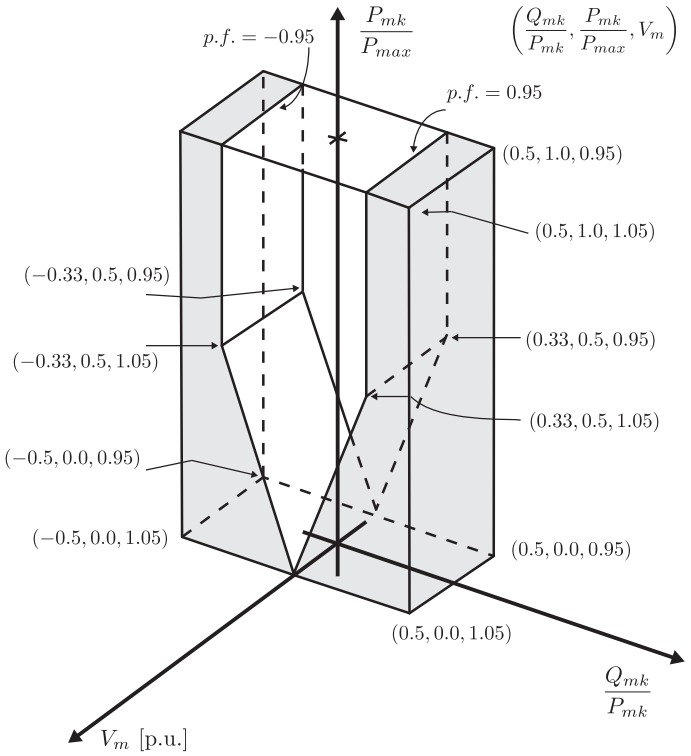

FIGURE 2.8: Diagram $\frac{Q_{mk}}{P_{mk}}, \frac{P_{mk}}{P_{max}}, V_m$ for asynchronous resources.

output of 0.5 P_{max}. and iii) the voltage magnitude V_m must be within its limits. The last two conditions are mathematically represented by

$$-0.33P_{mk} \leq \quad Q_{mk} \quad \leq 0.33P_{mk} \qquad 0.5P_{max} \leq P_{mk} \leq P_{max} \tag{2.56}$$

$$-\frac{0.33}{0.5}\frac{P_{mk}^2}{P_{max}} \leq \quad Q_{mk} \quad \leq \frac{0.33}{0.5}\frac{P_{mk}^2}{P_{max}} \qquad 0 < P_{mk} < 0.5P_{max} \tag{2.57}$$

$$V_{min} \leq V_m \leq V_{max} \tag{2.58}$$

where P_{max} is defined as $P_{max} = 0.93V_kI_{max}$, to accomplish the requeriments of reactive power. On the other hand, the minimum and maximum voltage magnitudes are $V_{min} = 0.95$ p.u. and $V_{max} = 1.05$ p.u., respectively. For the proposed approach, the inequality constraints (2.56) and (2.57) are merged into one single equality function representing the injection of reactive power in one of the two VSC's operating regions:

$$Q_{mk} = \chi 0.33P_{mk}\left[-\frac{P_{mk}}{0.5P_{max}}\kappa + (1-\kappa)\right] \tag{2.59}$$

where $\kappa \in \{0, 1\}$. This binary variable is calculated during the iterative process and permits the switching between functions (2.56) and (2.57) according with the

current value of P_{mk}. As shown in Fig. 2.7, when $\kappa = 1$ the VSC is operating in its upper region, the opposite takes place when $\kappa = 0$. On the other hand, the parameter χ controls the level of reactive power injected into the grid. Based on what was mentioned above and the proposed equation (2.59) is that the VSC's grid code control modes are derived from basic principles. Note that, the basic mistmach equations of the PV plant reported in Section 2.4.1 prevail for this new proposal, together with (2.46) and its associated state variable χ_s.

2.6.1.1 *MGC* PQ control mode

In this control mode (2.59) is modified as (2.60) in order to introduce the complementarity control variables ι_a and ι_b. The state variable associated to this equation is m_a.

$$\Delta u_{15} = Q_{mk} - (\chi - \iota_a + \iota_b)0.33P_{mk}\left[-\frac{P_{mk}}{0.5P_{max}}\kappa + (1-\kappa)\right] = 0 \quad (2.60)$$

$$\Delta u_{16} = \sqrt{\left[(V_m - V_{min}) - \iota_a\right]^2 + 4\mu^2} - \left[(V_m - V_{min}) - \iota_a\right] = 0 \quad (2.61)$$

$$\Delta u_{17} = \sqrt{\left[(V_{max} - V_m) - \iota_b\right]^2 + 4\mu^2} - \left[(V_{max} - V_m) - \iota_b\right] = 0 \quad (2.62)$$

Equations (2.61) and (2.62) represent the complementarity constraints to handle the voltage magnitud limits as well as their corresponding state variables denoted by ι_a and ι_a, respectively. Finally, $P_{lim} = P_{max}$.

2.6.1.2 *MGC* PQ control mode-fixed power factor

For this control mode, the reactive power support depends on the value of pf according to Fig 2.8. This dependency represented by expressing (2.60) as (2.63), where the parameter χ is replaced with the state variable χ_c. The state variable m_a is associated with (2.64). On the other hand, the complementarity constraints (2.65)-(2.66) and the state variables ϱ_a and ϱ_b maintain the pf within limits.

$$\Delta u_{18} = Q_{mk} - (\chi_c - \iota_a + \iota_b)0.33P_{mk}\left[-\frac{P_{mk}}{0.5P_{max}}\kappa + (1-\kappa)\right] = 0 \quad (2.63)$$

$$\Delta u_{19} = Q_{mk} - P_{mk}\tan(\text{acos}(pf)) - \varrho_a + \varrho_b = 0 \quad (2.64)$$

$$\Delta u_{20} = \sqrt{\left[(\chi_c - \chi_{min}) - \varrho_a\right]^2 + 4\mu^2} - \left[(\chi_c - \chi_{min}) - \varrho_a\right] = 0 \quad (2.65)$$

$$\Delta u_{21} = \sqrt{\left[(\chi_{max} - \chi_c) - \varrho_b\right]^2 + 4\mu^2} - \left[(\chi_{max} - \chi_c) - \varrho_b\right] = 0 \quad (2.66)$$

Lastly, constraints (2.61) and (2.62) are also considered in this control mode, while the active power limit is calculated as $P_{lim} = P_{max}$.

2.6.1.3 *MGC* PV control mode

Based on Sections 2.5.1.3 and 2.5.2.2, this operating mode controls the voltage magnitud V_m at the POI at a specified value V_{ref}. This control mode is mathematically composed of equations (2.46), (2.49), (2.50) and (2.51), while the active and reactive power limits are calculated by

$$P_{lim} = P_{max} \tag{2.67}$$

$$Q_{min} = 0.33P_{mk}\left[\frac{P_{mk}}{0.5P_{max}}\kappa + (1-\kappa)\right] \tag{2.68}$$

$$Q_{max} = 0.33P_{mk}\left[-\frac{P_{mk}}{0.5P_{max}}\kappa + (1-\kappa)\right] \tag{2.69}$$

Lastly, note that the voltage reference must be selected according to Fig 2.8: $0.95 \leq V_{ref} \leq 1.05$ p.u.

2.7 Generalized power flow formulation

The explicit inclusion of the PV plant model in the power flow problem is accomplished by grouping together the set of nodal active and reactive power mismatch equations, $\boldsymbol{\Delta P}$ and $\boldsymbol{\Delta Q}$, and the equations describing the PV plant operation: $\boldsymbol{\Delta g}$, is the set of basic equations of the PV plant, $\boldsymbol{\Delta h}$ and $\boldsymbol{\Delta \Phi}$ represent the mismatch equations of the switching and complementarity limit checking approach respectively. Finally $\boldsymbol{\Delta u}$ represents the mismatch equations for VSC's control strategies and control modes under Mexican's grid code. In this context, the generalized power flow problem is formulated by the set of equations given by (2.70). The PV plant equations are selected according to:

i) The VSC's control modes and the approach used for handling its power limits, as reported in Tables 2.1 and 2.2 where the abbreviations WLC, LCSA and LCCA denote without limit checking, limit checking by using the switching approach and limit checking by using the complementarity condition approach, respectively.

ii) The VSC's control strategies and their associated control modes are reported in Tables 2.3 and 2.4.

iii) The VSC's control modes under the Mexican's grid code are reported in Table 2.5

$$\boldsymbol{f}(\boldsymbol{x}) = [\boldsymbol{\Delta P}\ \boldsymbol{\Delta Q}\ \boldsymbol{\Delta g}\ \boldsymbol{\Delta h}\ \boldsymbol{\Delta \Phi}, \boldsymbol{\Delta u}]^T = \mathbf{0}. \tag{2.70}$$

The use of augmented equations for the power flow problem lends itself to a suitable formulation to solve the nodal voltages of the network, $\boldsymbol{x}_{nt}$, and the PV plant state variables, $\boldsymbol{x}_{pvp}$, simultaneously. In this context, the Newton-Raphson method is used to obtain an approximate solution to the nonlinear problem $\boldsymbol{f}(\boldsymbol{x}) = \mathbf{0}$, where $\boldsymbol{x} = [\boldsymbol{x}_{nt}\ \boldsymbol{x}_{pvp}]^T$, by solving for $\boldsymbol{\Delta x}^i$ in the i iteration solving the linear problem $\boldsymbol{J}^i \boldsymbol{\Delta x}^i = -\boldsymbol{f}(\boldsymbol{x}^i)$, where $\boldsymbol{J}$ is known as the Jacobian matrix. The method starts from an initial guess $\boldsymbol{x}^0$ and updates the solution for all state variables at each iteration i, i.e. $\boldsymbol{x}^{i+1} = \boldsymbol{x}^i + \boldsymbol{\Delta x}^i$, until a specified mismatch tolerance is satisfied: $\max \left| \boldsymbol{f}(\boldsymbol{x}^{\boldsymbol{i+1}}) \right| \leq TOL$.

TABLE 2.1: PV plant equations under a PQ operation mode

Approach	State variables	Equations
WLC	$I_{dc}, V_{dc}, m_a, \alpha$	(2.17), (2.18) (2.19), (2.20)
LCSA	$I_{dc}, V_{dc}, m_a, \alpha$ $P_{nom_{sv}}$ or ξ_s	(2.17), (2.23) (2.19), (2.20) (2.22)
LCCA	$I_{dc}, V_{dc}, m_a, \alpha$ ξ_c	(2.17), (2.32) (2.19), (2.20) (2.33)

TABLE 2.2: PV plant equations under a PV operation mode

Approach	State variables	Equations
WLC	$I_{dc}, V_{dc}, m_a, \alpha$	(2.17), (2.18) (2.19), (2.21)
LCSA	$I_{dc}, V_{dc}, m_a, \alpha$ $P_{nom_{sv}}$ or ξ_s Q_{vio} or V_{ref}	(2.17), (2.23) (2.19), (2.21) (2.22) (2.26)
LCCA	$I_{dc}, V_{dc}, m_a, \alpha$ ξ_c, v_a , v_b	(2.17), (2.32), (2.19), (2.34) (2.33), (2.35), (2.36)

TABLE 2.3: PV plant equations under Active power priority control strategy

Control Mode	State variables	Equations
PQ	$I_{dc}, V_{dc}, \alpha, I_{sh}$, ξ_s, m_a	(2.39), (2.40) (2.41), (2.42), (2.43), (2.44)
PQ (pf)	$I_{dc}, V_{dc}, \alpha, I_{sh}, \xi_s$, $m_a, \chi_s, \rho_a, \rho_b$	(2.39), (2.40) (2.41), (2.42) (2.43), (2.45), (2.46), (2.47), (2.48)
PV	$I_{dc}, V_{dc}, \alpha, I_{sh}, \xi_s$, m_a, v_a, v_b	(2.39), (2.40) (2.41), (2.42), (2.43), (2.49), (2.50), (2.51)

TABLE 2.4: PV plant equations under Reactive power priority control strategy

Control Mode	State variables	Equations
PQ	$I_{dc}, V_{dc}, \alpha, I_{sh}$, ξ_s, m_a	(2.39), (2.40) (2.41), (2.42), (2.43), (2.52)
PV	$I_{dc}, V_{dc}, \alpha, I_{sh}, \xi_s$, m_a, v_a, v_b	(2.39), (2.40) (2.41), (2.42), (2.43), (2.49), (2.50), (2.51)

TABLE 2.5: PV plant equations under the Mexican's grid code

Control Mode	State variables	Equations
PQ	$I_{dc}, V_{dc}, \alpha, I_{sh}$, $\xi_s, \chi_s, m_a, \iota_a, \iota_b$	(2.39), (2.40) (2.41), (2.42), (2.43), (2.46), (2.60), (2.61), (2.62)
PQ (pf)	$I_{dc}, V_{dc}, \alpha, I_{sh}, \xi_s$, $\chi_s, \iota_a, \iota_b, \chi_c, m_a$, ϱ_a, ϱ_b	(2.39), (2.40) (2.41), (2.42) (2.43), (2.46), (2.61), (2.62), (2.63) (2.64), (2.65), (2.66)
PV	$I_{dc}, V_{dc}, \alpha, I_{sh}, \xi_s$, χ_s, m_a, v_a, v_b	(2.39), (2.40) (2.41), (2.42), (2.43), (2.46), (2.49), (2.50), (2.51)

Finally, Fig. 2.9 is associated with the PV plant model when the switching approach is used for checking limits of the PV plant's state variables. Note that

when the limit checking is performed by the complementarity approach, the PV model is directly defined by the information reported in the third row of Tables 2.1 and 2.2 for the PQ and PV operating control modes, respectively.

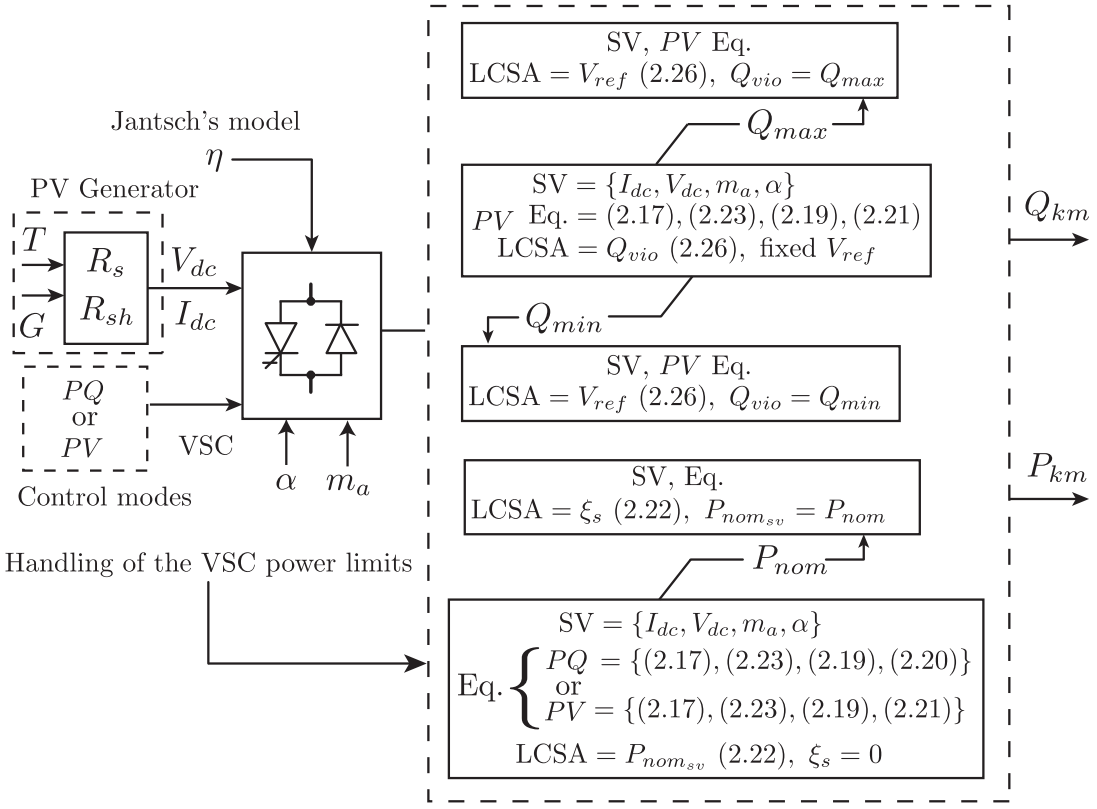

FIGURE 2.9: Block diagram of the PV plant model with LCSA

2.7.1 State variable initialization

The generalized unified power flow problem arrives at the solution with local quadratic convergence if proper initial conditions are given for the set of state variables. The flat initialization of nodal voltages is commonly used in conventional power flow studies [Acha et al., 2004], while the amplitude modulation ratio m_a is initialized at 1, and the VSC's phase angle α is set at 0°. On the other hand, the initialization of V_{dc} and I_{dc} is not a trivial task such that one way of defining their initial values consists of using the open circuit voltage V_{oc} and short circuit current I_{sc}, respectively, which are provided by manufacturer's datasheets at STC. Although these values provide a good estimate, this can be improved by selecting initial values of V_{dc} and I_{dc} closer to the MPP. This is achieved by first expressing I_{dc} as an explicit function of V_{dc}, or vice versa. This explicit function can be derived from (2.1) by using the Lambert W function [Lim et al., 2015], which results in

$$\begin{aligned} I_{dc} &= \frac{R_{sh}\left(I_{ph}+I_0\right)-V_{dc}}{R_s+R_{sh}} - \frac{V_t}{R_s} W\left\{\frac{R_s R_{sh} I_0}{V_t\left(R_s+R_{sh}\right)}\right. \\ &\times \left. \exp\left(\frac{R_{sh}\left(R_s\left(I_{ph}+I_0\right)+V_{dc}\right)}{V_t\left(R_s+R_{sh}\right)}\right)\right\}, \end{aligned} \tag{2.71}$$

where $W\{\cdot\}$ refers to the Lambert W function, which cannot be expressed in terms of elementary functions. Therefore, the series expansion employed to approximate $W\{\cdot\}$ is the one given in [Batzelis et al., 2014]. Based on (2.71), the dyad of I_{dc} and V_{dc} that provides the maximum value of P_{dc} can be obtained by computing a set of values for I_{dc} by varying V_{dc} from 0 to V_{oc}. The dyad $\{I_{dc}, V_{dc}\}$ associated with the maximum computed value of P_{dc} is then selected as an initial value for the state variables I_{dc} and V_{dc}, respectively.

2.8 Summary

This chapter proposes the paramater extraction of PV panel model in order to incorporate the equations representing the operation of a PV generator, together with those associated with the control laws of the VSC. The operational limits of the VSC are taking into account considering two novel approaches: switching approach and complementarity approach. Moreover a second formulation of the PV plant model is developed from basic principles, where the capability curve of the VSC is incorporated to the model. In this context, is proposed a practical

PV plant model to meet the requirements set by the Mexican's grid code for the interconection of PV plants. Lastly, the simultaneous solution of the state variables associated with the PV plant model together with the rest of the state variables of the electric power system is formulated in the context of the power flow problem.

Chapter 3

Case studies

3.1 Introduction

The developed power flow program, including the PV plant model with their respective control modes and operational limits described in Chapter 2, has been applied to the solution of two electric networks considering varying degrees of operational complexity. This Chapter presents the corresponding computational results to demonstrate the reliability of the proposed approach and the developed computer program.

3.2 Case studies

The performance of the proposed approach is evaluated by using the IEEE-14 bus test system and a real Mexican 71-bus power system. The proposed PV plant model and power flow algorithm were implemented in the MATLAB® platform, and the power flow studies were performed with a mismatch tolerance of 10^{-12} by considering either the switching or complementarity approach. For this purpose, the 330W Kyocera KU330-8BCA photovoltaic panel has been selected with its datasheet given in [Kyocera, 2014]. The panel's resistor values are $R_{sh} = 652.51\Omega$ and $R_s = 280.84\text{m}\Omega$. In both IEEE-14 and real Mexican 71-bus power system the reactive power limits were not considered for the conventional generators.

3.2.1 IEEE-14 test system

3.2.1.1 Base case

In this case, the conventional generator embedded at bus 6 is replaced by four parallel-connected PV power plants, Bus6-U1 to Bus6-U4, with their PV generators composed of an array of multiple panels as reported in Table 3.1, and the resistors values are $R_{sh} = 10.354\Omega$ and $R_s = 4.45\text{m}\Omega$. The parameters for each VSC are the same, with a nominal active power of $P_{nom} = 12.50$ MW, a droop control parameter of $K_p = 2 \times 10^{-3}$, an efficiency of $\eta = 98\%$ and power factor limits of $0.95 \leq pf \leq 1$. The transformer reactance for all PV units is $X_T = 0.9$ per-unit (p.u.). All power plants are operating at the PV control mode to set the voltage magnitude at the POI node at $V_{ref} = 1.08$ p.u. Similarly, these units operate under the same temperature of 28°C but at different levels of irradiance as shown in Table 3.2. The power flow study converged to the same solution in four and six iterations by using the switching and complementarity approaches, respectively, as shown in Fig. 3.1. Since no operating limit of the PV units was violated, the switching approach was not activated. On the other hand, the complementarity approach is always activated during the iterative process, whereby this approach always takes more iterations to obtain convergence when no limit violations have occurred during the iterative process. Lastly, the final values of the state variables associated with each PV unit are given in Table 3.2. Since each unit is operating under different levels of irradiance, the resulting $P_{dc} = V_{dc}I_{dc}$ achieved at the MPP is also different for each unit.

TABLE 3.1: PV generator parameters

STC Conditions ($T_n = 25°\text{C}$, $G_n = 1000\text{W/m}^2$)					
System	Parameter				
	P_{mpp}	I_{mpp}	V_{mpp}	N_{pp}	N_{ss}
IEEE-14 test system	12MW	12.3kA	0.97kV	1515	24
BCSPS	6.2MW	6.3kA	0.97kV	783	24

Table 3.2 also shows the final values of ηP_{dc}, Q_{km} and lagging pf for each single PV plant unit. Clearly, unit Bus6-U2 is operating closer to its STC: $P_{dc} \cong P_{mpp}$. On the other hand, Bus6-U4 operates with the lowest irradiance, which results in the lowest $\eta P_{dc} = 0.1090$ p.u. Note also that all PV units generate the same amount of reactive power to achieve the specified control of voltage magnitude: $Q_{km} = 0.0225$ p.u. The reason for this performance is because the voltage droop

controller has the same value of K_p for each PV unit. Lastly, the power factor at which each unit is operating is computed from (2.20).

3.2.1.2 Violation of VSCs' limits

In order to assess the performance of the proposed approach when violations exist in the VSCs' operation limits, the case study previously reported was repeated but with the levels of irradiance reported in Table 3.2, a temperature of 32°C and a control voltage magnitude at $V_{ref} = 1.1$ p.u. The same power flow solution was obtained by using any of the two proposed approaches for limit checking, with the state variable values of each PV plant reported in the last four columns of Table 3.2. From the analysis of these results, the non-null value of ξ indicates that units Bus6-U1 and Bus6-U2 violated their active power limits, i.e. they are no longer operating under MPP, whereby their active powers are fixed at P_{nom}. On the other hand, units Bus6-U3 and Bus6-U4 operate under the MPP mode with values of $\eta P_{dc} < P_{nom}$.

All PV plants have also violated their corresponding maximum reactive power limit such that all units operate at the PQ control mode at a fixed pf of 0.95, with their reactive power generation fixed at the violated limit. This limit is calculated for each PV unit by either using (2.25) for the switching approach or the merit function (2.36) for the complementarity approach. Since this limit's value depends on the active power supplied by the corresponding PV plant, units Bus6-U1 and Bus6-U2 supply the same reactive power generation because they have also been fixed at their maximum active power P_{nom}. In this case, the voltage magnitude's final value at node 6 was 1.093 p.u. instead of the target value of $V_{ref} = 1.1$ p.u.

Unlike the case study where no limit violations took place, the solution was obtained in seven iterations by using the complementarity approach, while two more iterations were required when the limit checking was carried out by the switching approach. Furthermore, the switching approach was applied by considering truncated adjustments in the state variables during the solution of (2.70) [Acha et al., 2004]; otherwise, the iterative process diverges. The convergence profile of the proposed generalized power flow for both limit handling approaches is shown in Fig. 3.1, where the discontinuity observed in the convergence trajectory associated with the switching approach is due to limits violation conditions.

TABLE 3.2: Values of state variables for IEEE-14 test system

PV plant units												
Parameters and state variables	No limits violation $T = 28°C$ Constant η				Limits violation $T = 32°C$ Constant η				Limits violation $T = 32°C$ Jantsch's model			
	Unit 1	Unit 2	Unit 3	Unit 4	Unit 1	Unit 2	Unit 3	Unit 4	Unit 1	Unit 2	Unit 3	Unit 4
G (W/m^2)	990	1000	950	930	1110	1120	970	980	1110	1120	970	980
V_{dc} (p.u.)	1.8758	1.8761	1.8746	1.8740	1.9930	2.0043	1.8712	1.8715	1.9930	2.0043	1.8712	1.8715
I_{dc} (p.u.)	0.0632	0.0638	0.0606	0.0593	0.0640	0.0636	0.0618	0.0625	0.0640	0.0636	0.0618	0.0625
α (degree)	-7.7628	-7.7575	-7.7841	-7.7948	-7.5157	-7.5157	-7.5659	-7.5607	-7.5154	-7.5154	-7.5655	-7.5604
m_a	0.9417	0.9416	0.9423	0.9427	0.8985	0.8934	0.9567	0.9566	0.8985	0.8934	0.9567	0.9566
$\xi_s = \xi_c$	0	0	0	0	0.0979	0.1115	0	0	0.0979	0.1115	0	0
P_{km} (p.u.)	0.1161	0.1173	0.1114	0.1090	0.1250	0.1250	0.1134	0.1146	0.1250	0.1250	0.1134	0.1146
Q_{km} (p.u.)	0.0225	0.0225	0.0225	0.0225	0.0411	0.0411	0.0373	0.0377	0.0411	0.0411	0.0373	0.0377
pf	0.9818	0.9822	0.9803	0.9794	0.9500	0.9500	0.9500	0.9500	0.9500	0.9500	0.9500	0.9500
η	0.9800	0.9800	0.9800	0.9800	0.9800	0.9800	0.9800	0.9800	0.9800	0.9800	0.9801	0.9801

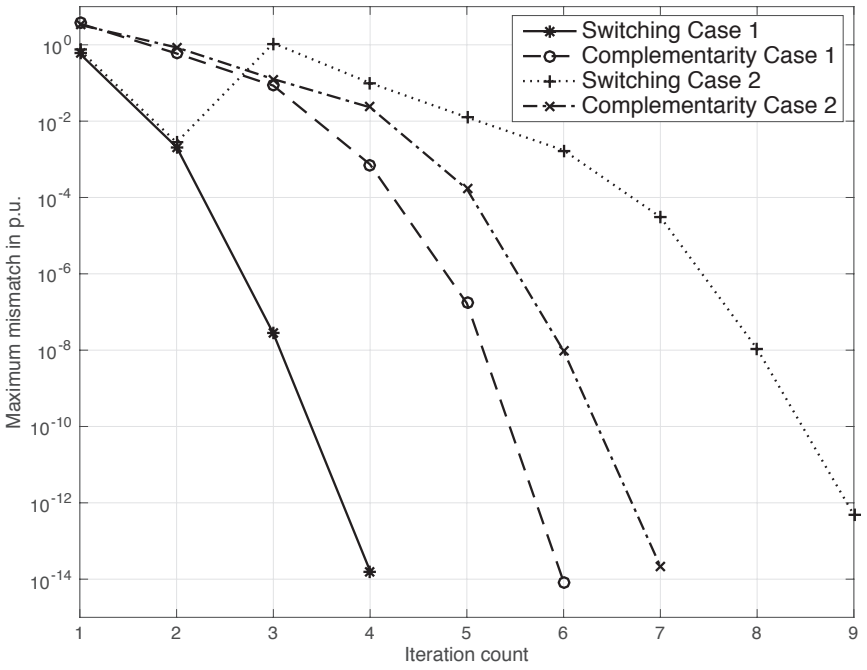

FIGURE 3.1: Convergence profile for both limit handling approaches.

3.2.1.3 Comparison of efficiency representation

The last simulation where the VSCs violated some of their operating limits has been repeated, but by considering the Jantsch model for representing the efficiency of converters [Monteiro et al., 2016]. The results are shown in the last four columns of Table 3.2. A comparison of these power flow results with respect to those obtained when using a constant value of efficiency clearly shows that both approaches give similar results. This is because of the output power at the VSCs' AC terminals.

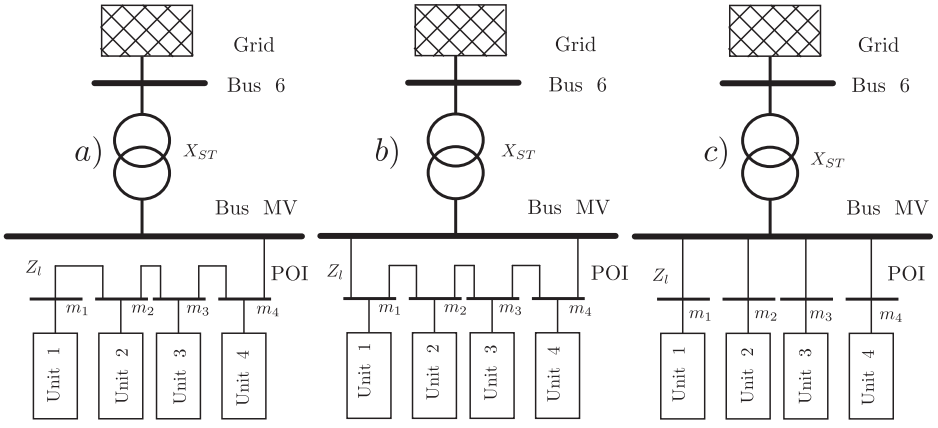

FIGURE 3.2: Collection grid topologies.

3.2.1.4 Collection grid topologies

The capability of the proposed approach to simulate different AC collection grid topologies is reported in this section. For this purpose, the simulation reported in Section 3.2.1.2 when violations of the VSC's operation limits take place has been newly repeated, but it considers the radial, ring and star collection grid topologies [Cabrera-Tobar et al., 2016]. In the former topology, the four PV units are connected to one feeder in one continuous string, as shown in Fig. 3.2 a). The ring topology derives from the radial topology by adding another feeder on the other side of the string, as shown in Fig. 3.2 b). Lastly, the star 1) topology is shown in Fig. 3.2 c) where each PV unit is connected to the main collector. In all these topologies, each PV unit is operating in the PV control mode to set the voltage magnitude at its corresponding medium voltage bus at $V_{ref} = 1.1$ p.u. All lines composing the topologies have the same impedance of $Z_l = 0.01335 + j0.04211$ p.u., while the same station transformer connecting nodes MV and HV has been considered for all topologies with a reactance of $X_{ST} = 0.25202$ p.u. The results obtained for the state variables of each generator are reported in Table 3.3 according to the type of AC collection grid topology considered in the power flow study. Each PV plant unit operates at lagging pf. The analysis of these results is similar to the one described in Section 3.2.1.2.

TABLE 3.3: Values of state variables for IEEE-14 test system with different AC collection grid topologies

	PV plant units											
Parameters and state variables	Limits violation $T = 32°C$ Radial configuration				Limits violation $T = 32°C$ Ring configuration				Limits violation $T = 32°C$ Star configuration			
	Unit 1	Unit 2	Unit 3	Unit 4	Unit 1	Unit 2	Unit 3	Unit 4	Unit 1	Unit 2	Unit 3	Unit 4
G (W/m^2)	990	1000	950	930	1110	1120	970	980	1110	1120	970	980
V_{dc} (p.u.)	1.9930	2.0043	1.8712	1.8715	1.9930	2.0043	1.8712	1.8715	1.9930	2.0043	1.8712	1.8715
I_{dc} (p.u.)	0.0640	0.0636	0.0618	0.0625	0.0640	0.0636	0.0618	0.0625	0.0640	0.0636	0.0618	0.0625
α (degree)	0.8819	0.6166	0.0807	-0.6085	-1.0914	-0.8657	-0.9302	-1.1526	-1.3886	-1.3886	-1.4138	-1.0935
m_a	0.8999	0.8984	0.9589	0.9533	0.9024	0.8971	0.9614	0.9606	0.9031	0.8981	0.9622	0.9620
$\xi_s = \xi_c$	0.0979	0.1115	0	0	0.0979	0.1115	0	0	0.0979	0.1115	0	0
P_{km} (p.u.)	0.1250	0.1250	0.1134	0.1146	0.1250	0.1250	0.1134	0.1146	0.1250	0.1250	0.1134	0.1146
Q_{km} (p.u.)	0.0210	0.0411	0.0373	0.0377	0.0411	0.0146	0.0205	0.0377	0.0288	0.0288	0.0321	0.0318
pf	0.9861	0.9500	0.9500	0.9500	0.9500	0.9932	0.9840	0.9500	0.9744	0.9744	0.9622	0.9637
η	0.9800	0.9800	0.9801	0.9801	0.9800	0.9800	0.9801	0.9801	0.9800	0.9800	0.9801	0.9801
POI, V_m (p.u.)	1.1	1.0994	1.0957	1.0894	1.0980	1.1	1.1	1.0978	1.1	1.1	1.1	1.1

3.2.1.5 Distributed PV generation

In this study, five PV plants of different power capabilities have been embedded in five different nodes of the system as reported in Table 3.4. The parameters and control mode of operation associated with each PV plant, as well as the power flow solution, are also reported in this Table. This solution indicates that units Bus7-U3 and Bus11-U4 violated their active power and reactive power limits, respectively. On the other hand, the rest of PV units remain operating within their power limits.

TABLE 3.4: Parameters and state variables for PV Plants

Parameters and state variables	PV plant units				
	Bus 5 Unit 1	Bus 6 Unit 2	Bus 7 Unit 3	Bus 11 Unit 4	Bus 14 Unit 5
T (°C)	21°	30°	35°	24°	26°
G (W/m^2)	600	980	1200	700	800
P_{nom} (MW)	15.5	48.5	7.5	30.5	8.5
X_T (p.u.)	0.3871	0.1237	0.800	0.1967	0.7059
R_s ($m\Omega$)	3.55	1.11	7.62	1.78	6.66
R_{sh} (Ω)	8.22	2.58	17.74	4.14	15.53
Control mode	PQ	PV	PQ	PV	PQ
V_{dc} (p.u.)	1.8609	1.8735	2.0411	1.8661	1.8703
I_{dc} (p.u.)	0.0478	0.2500	0.0375	0.1115	0.0340
α (degree)	-2.8651	-1.6227	-3.7106	-2.9863	-4.9238
m_a	0.9134	0.9415	0.8538	0.9561	0.9277
$\xi_s = \xi_c$	0	0	0.0975	0	0
P_{km} (p.u.)	0.0872	0.4591	0.0750	0.2040	0.0624
Q_{km} (p.u.)	0.0177	0.1270	0	0.0671	0.0182
V_m (p.u.)	1.0349	1.0800	1.0686	1.0811	1.0513
pf	0.9800	0.9996	1.0000	0.9500	0.9600
η	0.9801	0.9801	0.9800	0.9802	0.9802

3.2.2 71-bus electric power system

This electric power system shown in Fig. 3.5, referred to as Equivalent PS, is part of a real power system, and consists of 71 buses, 44 transmission lines, 44 two-winding and 3 three-winding transformers [Romero, 2014]. The generation portfolio is composed of steam plants, gas turbines and internal combustion generators. In 2016, solar energy represented 3.1% of the overall region capacity with 32 MW, but it is expected that this capacity will increase to 300 MW by 2031

[PRODESEN 2017, 2017]. This exponential growth is basically defined by its daily solar irradiance of 8.5 kWh/m^2, which results in several requests for integrating solar PV plants from private utilities. Based on the mentioned above, 15 PV plants have been embedded in the system at 115 kV nodes B50, B53 and B66, considering five parallel-connected power plants at each node, with the parameters of each single VSC similar to those reported in Section 3.2.1. The difference is that the nominal power is now $P_{nom} = 6.50$ MW. Furthermore, the set of Kyocera photovoltaic panels composing the PV generator, as well as the generator's characteristics, are given in Table 3.1, where the following values of resistances have been adopted: $R_{sh} = 20.033\Omega$ and $R_s = 8.61\text{m}\Omega$. Table 3.5 shows the weather conditions for each PV plant. Based on this information, two power flow studies have been performed, with and without the handling of limits, by considering that the set of PV plants connected at node B66 are operating in the PQ control mode. Similarly, the rest of the renewable generators are considered to be operating in the PV control mode to control the voltage magnitude at nodes B50 and B53 at 1.02 p.u. and 1.04 p.u., respectively. Regarding the set of generators embedded at node B66, units B66-U4 and B66-U5 operate at unity power factor, while units B66-U1, B66-U2 and B66-U3 operate at lagging power factors of 0.95, 0.98 and 0.96, respectively.

Table 3.5: Weather conditions of PV plants

PV plants at Bus 66			PV plants at Bus 53			PV plants at Bus 50		
	G	T		G	T		G	T
B66	W/m^2	°C	B53	W/m^2	°C	B50	W/m^2	°C
U1	920	34	U1	960	36	U1	975	36
U2	935	34	U2	920	34	U2	980	36
U3	970	35	U3	970	36	U3	1140	38
U4	1130	37	U4	1100	38	U4	970	35
U5	980	35	U5	1090	38	U5	1150	38

When no power limits were considered in the power flow study, the specified control actions were achieved. On the other hand, when limits were checked only the voltage magnitude at node B53 was controlled. In this case, the five units embedded at this node were able to perform the control action, but units B53-U4 and B53-U5 violated their corresponding active power limit P_{nom}. In contrast, all generators embedded at node B50 violated their maximum reactive power limit, and units B50-U3 and B50-U5 also violated their active power limits. Lastly, unit B66-U4 operating in PQ control mode has also violated its active power limit.

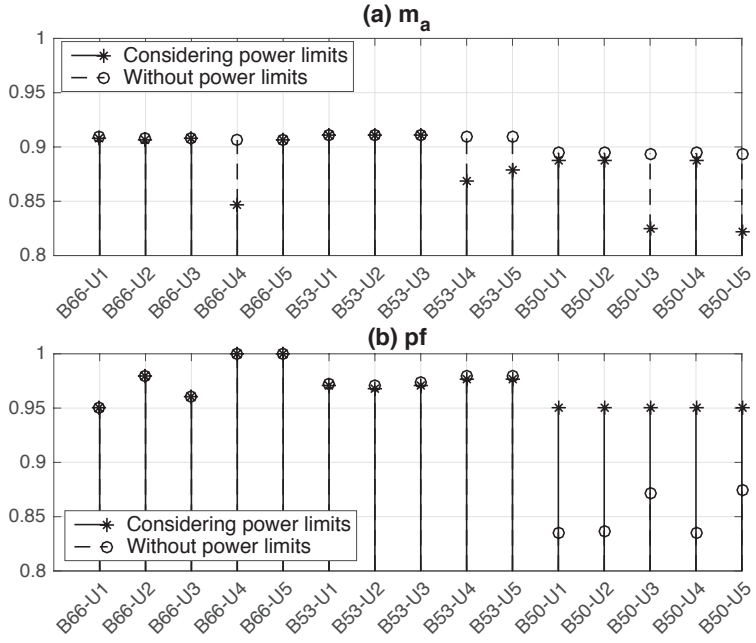

FIGURE 3.3: m_a and pf for each unit.

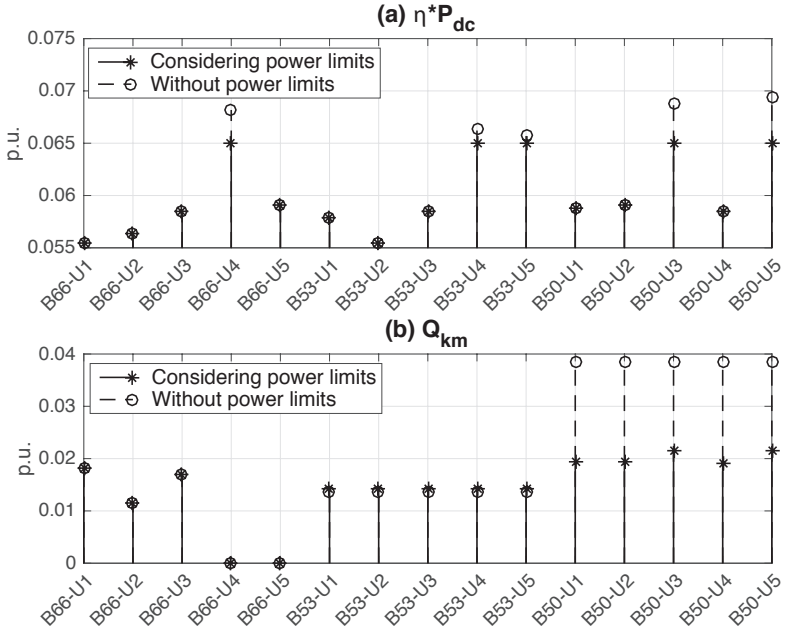

FIGURE 3.4: Active and reactive power generation by PV units.

Figure 3.3 (a) shows the value of m_a for each VSC unit for both case studies. Note that the value of m_a became lower when the active power limit was violated; this is because the PV plant is no longer operating in the MPP. In addition, there was an increment in the voltage value at the DC side of the VSC. For the units that only violated the reactive power limit (B50-U1,U2 and U4), m_a had a slight change. When power limits were not considered, the units B50-U1 to B50-U5 worked at

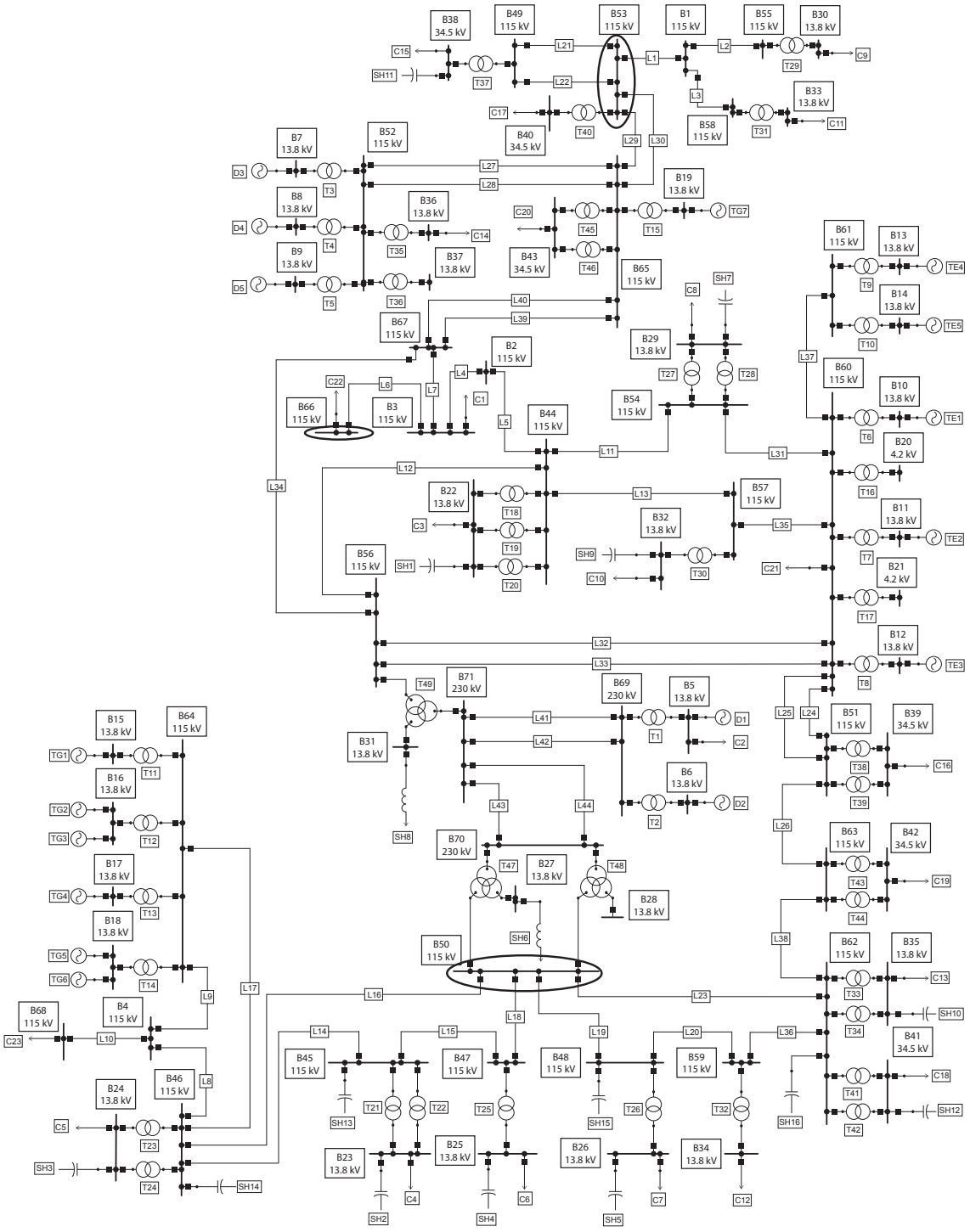

FIGURE 3.5: Equivalent portion of a real power system.

a lower pf than allowed for the VSC, as shown in Fig. 3.3 (b). On the other hand, when these limits were considered the pf was fixed at the maximum value allowed for the VSC, and a slight change in the pf of units B53-U1 to B53-U5 is accomplished.

Figure 3.4 (a) shows the AC power ηP_{dc} for each unit, where it is observed that B66-U4, B53-U4, B53-U5, B50-U3 and B50-U5 were fixed at $P_{nom} = 0.065$ p.u. Similarly, Fig. 3.4 (b) shows the reactive power of all PV units involved in the study. When the power limits were not considered, units B50-U1 to B50-U5 were dispatched at the same value, and the voltage magnitude was controlled at the target value. On the contrary, when limits were checked, the Q_{km} produced by these units was imposed according to the generation of active power at a fixed pf. In this case, the uncontrolled voltage at bus 50 was $V_{B50} = 1.0132$ p.u.

3.2.3 Comparison to other proposals

The case studies reported in references [Ahmed and Mohsin, 2011] and [Kamh and Iravani, 2012] have been reproduced in this section to compare our proposal with respect to the models where PV solar parks are modeled by equivalent generators. In accordance to these references, it is considered that the solar park is composed of one single PV plant. Table 3.6 reports the values of state variables associated with the PV plant embedded at node 3 of the 5-bus test system. The proposal reported in [Ahmed and Mohsin, 2011] is modeled and validated using DIgSILENT. A comparison of these results clearly shows that the solution obtained by our proposal is similar to the one reported in [Ahmed and Mohsin, 2011]. Due to the value of α in [Ahmed and Mohsin, 2011] is obtained before the power flow analysis and its variation is assumed linear when the power flow study is performed, the final value of this this state variable is slightly different with respect to the one given by our proposal.

On the other hand, the model in [Kamh and Iravani, 2012] is implemented in MATLAB® and validated against PSCAD/EMTDC. A similar conclusion is reached after comparing the results obtained by our proposed approach with respect to those reported in [Kamh and Iravani, 2012], which are shown in Table 3.7. Note that the values of the modulation index reported in Table 3.7 of [Kamh and Iravani, 2012] correspond to the voltage magnitudes at the AC inverter's terminal. This was verified by using the set of equations (10)-(15) given in this reference. Note that in Tables 3.6 and 3.7 the PV plants operate at lagging pf.

TABLE 3.6: Results for the 5-bus test system

α	m_a	V_k	pf	P_{km}	Q_{km}
Model [Ahmed and Mohsin, 2011]					
2.882	0.8426	1.032	0.9942	0.48	0.052
Proposed approach					
3.1223	0.8400	1.0240	0.9942	0.48	0.0519

TABLE 3.7: Results for the 12-bus test system

	V_m	m_a	V_k	pf	P_{mk}	Q_{mk}
Model [Kamh and Iravani, 2012]						
Unit 1	0.9071	0.9163	0.8997	0.9	0.5345	0.2588
Unit 2	0.9074	0.9166	0.9000	0.9	0.5346	0.2589
Unit 3	0.9072	0.9164	0.8998	0.9	0.5345	0.2588
Proposed approach						
Unit 1	0.9071	0.9107	0.8997	0.9	0.5345	0.2583
Unit 2	0.9074	0.9110	0.9000	0.9	0.5345	0.2583
Unit 3	0.9072	0.9108	0.8998	0.9	0.5345	0.2583

3.3 Case studies considering the VSC's Capability

3.3.1 IEEE-14 test system

In this study, a multiple collection configuration [Cabrera-Tobar et al., 2016] is connected at buses 6, 10, 11 and 14, respectively. The conventional generator embedded at buses 6 is replaced by 4 PV plants, which are connected in a start 2) configuration as shown in Fig 3.6 for the four units 1 to 4 with the POI at bus 6. On the other hand, 4 and 2 PV plants are connected at buses 10 and 1,1 respectively, considering a start 1) collection topology, which is shown in Fig. 3.2 c). Lastly, 2 PV plants are also connected at bus 14 considering a star 2) configuration. The ideal transformers connecting the PV plants to buses 6 and 10 have a reactance values of 0.48 p.u. and 0.8 p.u., respectively; while the other transformers embedded at buses 11 and 14 have a reactance of 0.7059 p.u. The temperature and irradiance are different for all PV plants involved in this study, as shown in Table 3.8. The abbrevations APP and RPP denote Active Power Priority and Reactive Power Priority. The following parameters are also reported in this Table: $R_s, R_{sh}, N_{pp}, N_{ss}, I_{max}$ and the control mode of each PV plant. Note that for this case study all control strategies and their corresponding control modes detailed in Section 2.5 are analyzed. The parameter of the droop control is given by $K_p = 2 \times 10^{-3}$; while the parameter corresponding to the complementarity merit function is $\mu = 1 \times 10^{-6}$. The mismatch tolerance was set on 10^{-6}. It need to take into account that the mismatch equations not only, involve active and

reactive power but also, DC voltage and current, and complementarity variables. This mainly justifies the use of this value of tolerance. Lastly, the power flow results associated with values of powers and state variables of each PV plant are reported in Table 3.8.

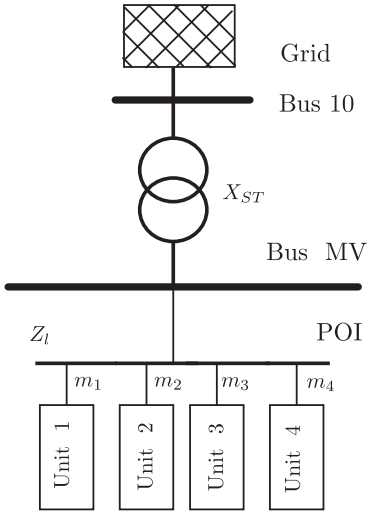

FIGURE 3.6: Star 2) topology.

From the set of data mentioned above PV plants at bus 6 are operating under the control strategy *APP* with a *PV* control mode to set the voltage magnitude at the POI node at $V_{ref} = 1.03$ p.u.. In this case, all power plants participate to achieve the control of voltage magnitude at its reference value by absorbing the same amount of reactive power: $Q_{km} = -0.0120$ p.u. The reason for this performance is because the voltage droop controller has the same value of K_p for each PV unit. The current through each VSC is maintained within limits, i.e. $I_{sh} \leq I_{max}$, as reported in Table 3.8; while all converters are operating at a leadding pf of nearly 0.98.

The four PV plants connected at bus 10 operate in a control strategy *APP*, where Units 1 and 3 are operating under a *PQ* control mode while Units 2 and 4 in a control mode *PQ*-fixed power factor (*PQ (pf)*). The weighting factor χ for units Unit 1 and 3 is set at 0.5 and 0.0, respectively, which means that Unit 3 does not injects reactive power to the grid. On the other hand, Unit 1 injects 0.0290 and operates to a pf of 0.911. Regarding other two PV plants, the requirement of operation for Units 2 and 4 is set at a lagging $pf = 0.95$. Due to the low level of solar irradiance at the geographical zone at which Unit 2 is located, its generation of active power is lower than the one generated by Unit 4 that is located in an area with high solar irradiance. Unit 2 is able to maintain its operation to the specified pf, however, which does not ocurr with Unit 4. In this case, the weighting factor

χ_s of Unit 4 is fixed at its upper limit 1. Furthermore, the final value of pf is 0.9739 instead of the target value 0.95. Note also that the VSC's current I_{sh} is equal to I_{max}, which means that the full VSC's capability is used.

The units connected at bus 11 are working under a RPP control strategy. Unit 1 operates in a PQ control mode, with $\chi = 0.7$. Because the irradiance in this area is good enough the active power must be curtailed in order to use the 70% of the VSC's capability to injected reactive power into the grid. Note that the VSC's current I_{sh} is equal to I_{max}, which means that the converter is operating to its full capability. The second Unit works in a PV control mode considering $\chi = 0.8$ for the reactive power limits, i.e. (2.54) and (2.55), and $V_{ref} = 1.07$. Similarly to the control action performed in Unit 1, the active power is curtailed but in this case the amount of both reactive power limits Q_{min} and Q_{max} is 80% of the S_{km}^{max}. The results show that Unit 2 achieves the voltage magnitude control at the system's POI.

Finally, two Units operating in a control strategy APP and PV control mode are connected at bus 14. The voltage reference V_{ref} is set at 1.03 p.u. for both Units. Note that the solar irradiance received by both units is high; therefore, the operating interval of the VSC's reactive power is low. This constrained reactive power operating range provokes that both Units violate their lower power limit such that the voltage magnitude at their POIs is now $V_m = 1.0373$, instead of $V_m = 1.03$, at the end of the solution process. Note that this result validates the implementation of the proposed approach because the converter is unable to absorb more reactive power to decrease the voltage magnitude; hence, the voltage magnitude at the POIs is higher than the one specified. This also causes that both PV plants units operate at full capacity: $I_{sh} = I_{max}$. Lastly, the amount of reactive power Q_{km} injected into the grid for both Units is different because there is no voltage control at the POI.

TABLE 3.8: Values of state variables for IEEE-14 test system

	PV plant units											
Parameters and state variables	*APP* Bus 6				*APP* Bus 10				*RPP* Bus 11		*APP* Bus 14	
	Unit 1	Unit 2	Unit 3	Unit 4	Unit 1	Unit 2	Unit 3	Unit 4	Unit 1	Unit 2	Unit 1	Unit 2
G (W/m^2)	1000	900	850	810	850	730	700	1150	900	955	1080	1070
T(°C)	32	30	33	35	32	24	28	39	33	34	33	34
R_s and R_{sh}	4.45$m\Omega$ and 10.354Ω				7.62$m\Omega$ and 17.744Ω				6.67$m\Omega$ and 15.531Ω		6.67$m\Omega$ and 15.531Ω	
N_{pp} and N_{ss}	1515 and 24				884 and 24				1010 and 24		1010 and 24	
I_{max} (p.u.)	0.125	0.125	0.125	0.125	0.0750	0.0750	0.0750	0.0750	0.0850	0.0850	0.0850	0.0850
Control mode	*PV*	*PV*	*PV*	*PV*	*PQ*	*PQ (pf)*	*PQ*	*PQ (pf)*	*PQ*	*PV*	*PV*	*PV*
V_{dc} (p.u.)	1.9916	1.9902	1.9844	1.9799	1.9856	1.9875	1.9803	1.9878	2.2262	2.1909	1.9926	1.9913
I_{dc} (p.u.)	0.0599	0.0539	0.0509	0.0485	0.0297	0.0255	0.0245	0.0402	0.0262	0.0304	0.0432	0.0427
α (degree)	6.1732	5.8651	5.7018	5.5723	0.6008	0.2893	0.2325	1.4659	-2.1013	-1.6707	2.6001	2.5731
m_a	0.8387	0.8396	0.8421	0.8441	0.8978	0.8903	0.8818	0.8924	0.8214	0.8023	0.8369	0.8360
P_{km} (p.u.)	0.1170	0.1052	0.0990	0.0940	0.0578	0.0497	0.0475	0.0782	0.0571	0.0653	0.0843	0.0834
Q_{km} (p.u.)	-0.0120	-0.0120	-0.0120	-0.0120	0.0290	0.0183	0.0000	0.0227	0.0761	0.0111	-0.0208	-0.0235
V_m (p.u.)	1.0300	1.0300	1.0300	1.0300	1.0712	1.0707	1.0700	1.0711	1.0723	1.0700	1.0373	1.0373
I_{sh} (p.u.)	0.1150	0.1035	0.0974	0.0926	0.0592	0.0489	0.0444	0.0750	0.0850	0.0616	0.0850	0.0850
χ or χ_s	N/A	N/A	N/A	N/A	0.5	0.2841	0	1.0	0.7	0.8	N/A	N/A
pf POI	-0.9879	-0.9869	-0.9862	-0.9856	0.9110	0.9500	1.0	0.9739	0.6265	0.9917	0.9557	0.9460

3.3.2 71-bus electric power system

For this case study, the interconnection of the PV plants must accomplish, not only with the Mexican Grid Code, but also with the VSC's capability current I_{sh}. In this context, the performance of the three proposed control modes is evaluated under the following assumptions:

i) The collection configuration used to interconnect several PV plants to any system's node has a start 1) topology, as schematically shown in Fig. 3.2.

ii) A set of four PV plants is connected at nodes 50, 53 and 60, respectively. Each PV plant's converter has a maximum current capacity of $I_{max} = 0.065$.

iii) Since all PV units must satisfy the Mexican's grid code requirements, no control strategy of operation is defined. A control mode of operation has to be specified, however, for each PV plant. In this context, all units embedded at node 50 operate under a PV control mode to set the voltage magnitude at a fixed value of $V_{ref} = 1.02$ p.u.. A *PQ (pf)*, control mode is selected for each unit connected at bus 53 with power factors of lagging 0.95, 0.95, 0.96 and 0.96 for units 1, 2, 3 and 4, respectively. Lastly, all units connected at bus 66 operate under a PQ control mode. In this case, the weighting parameter χ for units 1, 2, 3 and 4 is 0.5, 1.0, 0.7 and 0.6, respectively.

iv) Lastly, the levels of solar irradiance and temperature at each geographical area where each set of PV plants is located are reported in Table 3.9. Due to each set of PV plants is located in a large size area, the units composing each power plant are subjected to different solar irradiance and temperature.

Table 3.9: Weather conditions of PV plants Base case

PV plants at Bus 50			PV plants at Bus 53			PV plants at Bus 66		
	G	T		G	T		G	T
B50	W/m^2	°C	B53	W/m^2	°C	B66	W/m^2	°C
U1	890	32	U1	1350	32	U1	860	32
U2	870	30	U2	980	28	U2	1250	30
U3	950	33	U3	940	31	U3	850	33
U4	920	35	U4	1040	29	U4	930	35

3.3.2.1 Base case study

A power flow study is performed considering all parameters and assumptions mentioned above. These results show that the control of voltage magnitude at their corresponding POIs was achieved by the PV plant units connected at bus 50, while maintaining their pfs above 0.9496, which is the limit established in the Mexican grid code. On other hand, the converters' current I_{sh} is lower than I_{max}. These results are presented in Table 3.10.

For the PV plants connected at bus 53, the control mode corresponds to the *PQ (pf)*. In this case, Unit 1, Unit 2, and Unit 4 are not able to maintain their operation at the specified power factor. This is mainly due to the value of voltage magnitude at the POIs are higher than the limit imposed by the grid code: 1.05 p.u. In this context, the voltage magnitudes V_m are fixed at 1.05 p.u., and the pf is relaxed to values above those specified in order to absorb more reactive power. Nevertheless, Unit 3 maintains its operating status at a $pf = 0.96$ with V_m nearly close to 1.05 p.u. Note that converters of units 1 and 4 are operating with currents close to I_{max}, which means the VSCs are operating almost at full capacity. In this context, Unit 1 is under the mayor irradiance level producing such amount of active power that must be curtailed in order to accomplish the reserve of reactive power established in the grid code. All these results are reported in Table 3.10 . Finally, PV plants connected at bus 66 are working under PQ control mode. Similarly to Unit 1 at Bus 53, Unit 2 is also under a high irradiance. The parameter χ is equal to 1.0 and $P_{km} = P_{max}$, which means that a reduction of active power was made in order to have enough reactive power to achieve the requirements of the grid code. In this sense, $I_{sh} = I_{max}$ for this unit and the value of pf is the highest permited. The rest of units work under normal operation, with currents through their VSCs close to 0.05 p.u.. Table 3.10 also shows the value of κ, which indicates the operating zone of each PV plants, i.e. Upper or Lower Zone according to Fig. 2.7.

3.3.2.2 Reduction of solar irradiance in 45%

In this case study, the power flow simulation reported in the last section is newly repeated but considering that the solar irradiance captured by each PV plant is reduced in 45%, which means that these plants will produce less active power. In this context, and unlike the base case, the PV plants connected at bus 50 cannot be able to control the voltage at their POIs so that the voltage magnitudes are about

$V_m = 1.038$, as shown in Table 3.10. The physical explanation of this behavior is that the PV plants are operating in the Lower Zone of the Mexican's grid code curve, shown in Fig. 2.7, because the reduction in the active power output. In this operating zone, the interval of adjustment of reactive power to achieve a specified voltage magnitude control is significantly reduced, which produces the violation of converters' limits. On the other hand, the value of pf is slightly greater than 0.95 for for all converters, except the one associated with Unit 3 that is fixed at the $pf's$ limit. The PV plants at bus 53 operating under a *PQ (pf)* control mode maintain their pf at their respective preselected values. The voltage profile for these units is about $V_m = 1.037$ p.u.. Lastly, Units 1, 2 and 4 are operating in their Upper Zone, unlike Unit 3. All PV plants embedded at bus 66 are operating within limits, despite Units 1, 3 and 4 operate at their Lower Zone and with slightly different pf among each other. Note also that Unit 4 remains operating at its Upper Zone but with a different active power output with respect to the one obtained in the base case study. All these results are shown in Table 3.10.

3.3.2.3 Reduction of solar irradiance in 60%

In this case study all PV plants are operating in Lower Zone of the corresponding Mexican's grid code curve, except Unit 1 that is connected at bus 53. Similarly to the previous simulation, PV plants at bus 50 cannot control the voltage magnitude at their corresponding POIs. In this sense, the voltage magnitude at all POIs is 1.006 p.u. and the converters are operating with a pf about 0.97. Furthermore, the current flowing through these converters is around 0.02 p.u. that corresponds to the 30% of I_{max}. Regarding the PV plants connected at bus 53, Unit 1 is the only one that maintains its operation at a pf of 0.95, the rest of units are operating at a pf about 0.97. Since Unit 1 is operating in its Upper Zone, the current flowing through its converter is higher than those flowing through the other VSCs. Lastly, the PV plants connected at Bus 66 are operating within limits.

TABLE 3.10: Values of state variables for Baja California Sur power System Mexican Grid's Code

Parameters and state variables	PV Plants units at Bus 50				PV Plants units at Bus 53				PV Plants units at Bus 66			
	Unit 1	Unit 2	Unit 3	Unit 4	Unit 1	Unit 2	Unit 3	Unit 4	Unit 1	Unit 2	Unit 3	Unit 4
Control Mode	*PV*	*PV*	*PV*	*PV*	*PQ (pf)*	*PQ (pf)*	*PQ (pf)*	*PQ (pf)*	*PQ*	*PQ*	*PQ*	*PQ*
Base case												
V_m (p.u.)	1.0200	1.0200	1.0200	1.0200	1.0500	1.0500	1.0498	1.0500	1.0365	1.0372	1.0366	1.0367
I_{sh} (p.u.)	0.0542	0.0532	0.0574	0.0557	0.0634	0.0592	0.0563	0.0622	0.0506	0.0650	0.0506	0.0550
pf	0.9704	0.9675	0.9783	0.9744	0.9679	0.9556	0.9600	0.9648	0.9866	0.9496	0.9743	0.9809
κ	0	0	0	0	0	0	0	0	0	0	0	0
Reduction of solar irradiance in 45%												
V_m (p.u.)	1.0138	1.0138	1.0139	1.0139	1.0374	1.0371	1.0370	1.0371	1.0122	1.0128	1.0123	1.0123
I_{sh} (p.u.)	0.0297	0.0290	0.0319	0.0307	0.0451	0.0324	0.0306	0.0341	0.0277	0.0428	0.0276	0.0302
pf	0.9558	0.9575	0.9499	0.9531	0.9500	0.9500	0.9600	0.9600	0.9890	0.9496	0.9794	0.9817
κ	1	1	1	1	0	0	1	0	1	0	1	1
Reduction of solar irradiance in 60%												
V_m (p.u.)	1.0067	1.0067	1.0068	1.0068	1.0285	1.0282	1.0281	1.0282	0.9992	0.9997	0.9992	0.9993
I_{sh} (p.u.)	0.0208	0.0203	0.0224	0.0215	0.0326	0.0228	0.0217	0.0243	0.0198	0.0310	0.0197	0.0216
pf	0.9763	0.9773	0.9730	0.9748	0.9500	0.9721	0.9745	0.9686	0.9942	0.9524	0.9891	0.9903
κ	1	1	1	1	0	1	1	1	1	1	1	1

3.3.2.4 Comparision of Power Injected by the PV Plants and their impact on the system

This section presents a comparison of the results reported in the previous subsections where different levels of solar irradiance were considered. Figure 3.7 shows the active power P_{mk} injected for each PV plant at Buses 50, 53 and 66 for the three levels of irradiance describe above. The ordinate axis represent the real power injected in MW for each PV plant at its POI. On the other hand, the abscissa axis is associated with PV the set of units composing a PV power plant. Note that this set is repeated three times in each Figure because the three different levels of solar irradiance. The circle marker represents the active power injection of each PV plant when subjected to the base irradiance, the triangle and square marker are associated with the reduction of irradiance in 45% and 60%, respectively. As expected, the active power output of each PV plant is a direct function of the solar irradiance at the geographical area in which the plant is located.

Regarding the PV units connected at bus 50, for the three scenarios of solar irradiance it is Unit 3 that injects more active power than the rest units composing the solar park. A similar observation applies for the solar parks connected at buses 53 and 66, respectively. In the former (latter) Unit 1 (2) is the one that injects more active power into the grid. Note also that for all solar irradiation scenarios, the generation pattern followed by the PV units making up a solar park is similar.

Figure 3.8 shows the reactive power Q_{mk} injected MVARs into the grid for the three different scenarios of solar irradiance. Note that unlike the generation of active power, the generation pattern of reactive power changes with the level of solar irradiance. This is due to a change in active power generation has a direct effect on the zone of the Mexican's grid code curve in which the converters are operating, which affects converters' control mode of operation. By way of example, the results associated with the base case for the solar park connected at bus 50 clearly show that the maximum injection of reactive power is given by units 2, 3 and 3 for the scenarios of full irradiance, a reduction of 45% of irradiance and a 60% of reduction in the irradiance, respectively. The same type of observation also applies for the other solar parks. From this results it is also possible to deduce that the generation pattern of reactive power units composing a solar park does not change between different scenarios of solar irradiance if each unit remains operating in the same zone of the Mexican's grid code curve.

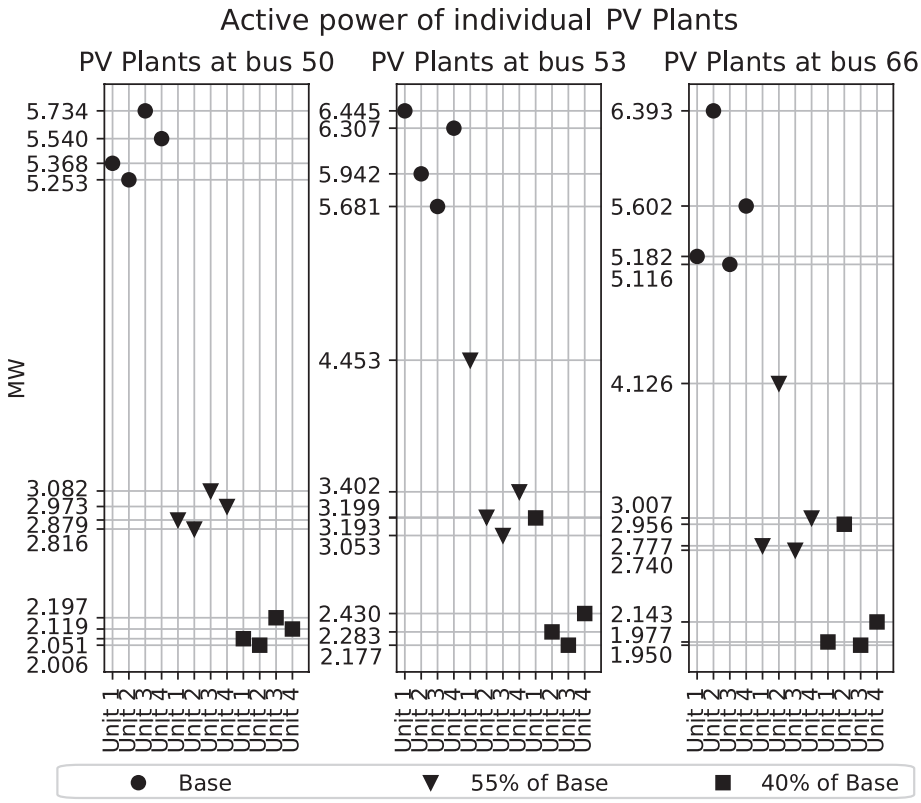

FIGURE 3.7: Active Power P_{mk} injected for Case Base, and reduction of 45% and 60% of solar irradiance.

Even though the individual injections of active (P_{mk}) and reactive (Q_{mk}) power were analyzed, it is important to evaluate the impact of the PV plants in the system's operation. In order to achieve this objective, the total active and reactive power injection of the PV plants is compared with respect to the power injected by the Slack bus. Figure 3.9 shows the existing relationships between the power generated by the solar parks and slack generator. As expected, this results clearly show how the latter compensates the variables of power generation of the solar parks because the changes in solar irradiance. Furthermore, these results also show that for the given specifications of the control mode of operation, the patterns of active and reactive power generation are opposite each other. Note that the interval of adjustment of reactive power increases with the reduction in the generation of active power. This indicates that the full capability of VSCs can be used to provide ancillary services associated with the control of voltage magnitude profiles when there is no solar irradiance.

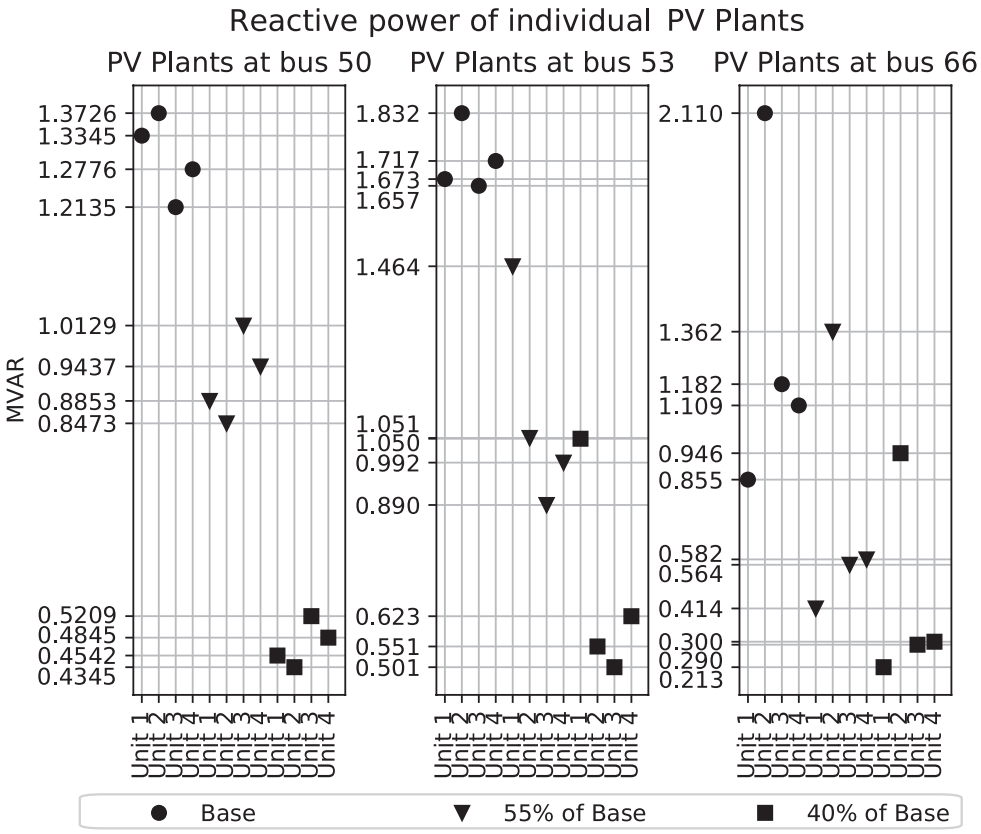

FIGURE 3.8: Reactive Power Q_{mk} injected for Case Base, and reduction of 45% and 60% of solar irradiance.

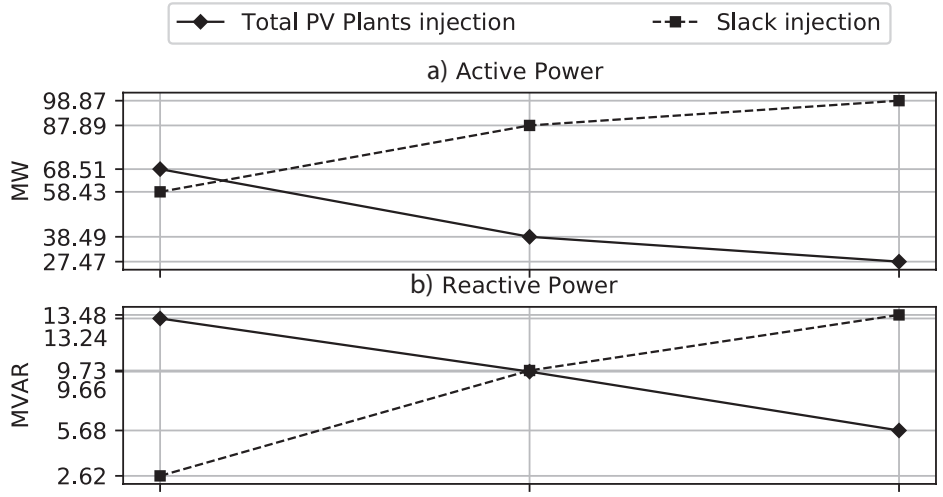

FIGURE 3.9: A comparison of active and reactive power generated by solar parks and slack bus.

3.4 Summary

In this chapter the PV plant, the control strategies and control modes were evaluated in two power systems. These simulations present the operation of the model and the control laws that govern the VSC under different scenarios of solar irradiance. On the other hand, the model has also been applied in a real-life system. In this sense, the PV plant model accomplishes with the criteria established in the Mexican's grid code. All these numerical simulations have been demostrated the suitability and applicability of the proposed approach.

Chapter 4

General conclusions and suggestions for future research work

4.1 General conclusions

A detailed grid-connected PV power plant model that considers both operation and control mode constraints has been proposed in this thesis for power flow analysis. In contrast to the existing methods, the proposed model offers:

- The directly incorporated in a Newton-based power flow program where the state variables of the PV plant are combined with the nodal voltages of the entire network for a unified iterative solution.
- The complementarity condition approach was used to directly introduce the set of PV plant constraints in the formulation of the power flow problem. This is rather attractive because the check of limits is simultaneously and automatically performed for all variables during the iterative power flow solution process.
- A switching approach was also proposed for checking limits, where the dimension of the power flow Jacobian matrix remains unaltered during the iterative solution process.

- The PV plant model was adequated to handle two control strategies, namely Active Power Priority and Reactive Power Priority, which take into account the VSC's capability curve.

- Three main control modes were developed to accomplish with the requirements of interconnection describe in the Mexican's grid code.

- Since reliability towards the convergence is of the utmost concern when using the Newton method, guidelines for the suitable initialization of the PV plant state variables have been provided. Lastly, the effectiveness of the proposed model and solution method has been fully validated by comparing the numerical results with respect to the ones reported in [Ahmed and Mohsin, 2011] and [Kamh and Iravani, 2012] .

4.2 Suggestions for future research work

Departing from the PV plant models and power flow solution approach proposed in this work, new proposals for future research work are detailed below

- To include the reactive power limits in the synchronous generators in an unified frame. Analyze the interaction between the high penetration of PV plants and the synchronous generators in the power system.

- The control strategies referred to as Active and Reacive Power Priorities can be reformulated in order to directly apply current control strategies. In this sense, the active and reactive power can be independently controlled by decomposing I_{sh} into i_d and i_q. This suggestion offers more flexibility to handle not only the active and reactive power injected, but also their corresponding operational limits.

- To extend the power flow analysis to an optimal power flow considering the PV plant under active and reactive power priority strategies. In this context, the PV plant can be can be dispatched to accomplish an optimal solution, while satisfying the Mexican grid code requirements.

- In order to have more information of the collection grid topologies, it is recommended to realize extensive simulations under different control strategies, control modes and weather contions. These simulations will permit to know which is the topology that offers the better performance.

- To implement efficient computer solutions in order to extend the power flow studies to real time applications.
- To develop a PV plant model for dynamic power flow studies. Since dynamic studies need a close initilization, this work can be useful for this purpose. The dynamic PV plant model can be integrated with a battery storage in order to regulate frequency.

Bibliography

Acha, E., Fuerte-Esquivel, C. R., Ambriz-Perez, H., and Angeles-Camacho, C. (2004). *FACTS: Modelling and Simulation in Power Networks*. John Wiley & Sons.

Ahmed, S. and Mohsin, M. (2011). Analytical determination of the control parameters for a large photovoltaic generator embedded in a grid system. *IEEE Transactions on Sustainable Energy*, 2(2):122–130.

Batzelis, E., Routsolias, I., and Papathanassiou, S. (2014). An explicit pv string model based on the lambert w function and simplified mpp expressions for operation under partial shading. *IEEE Transactions on Sustainable Energy*, 5(1):301–312.

Cabrera-Tobar, A., Bullich-Massagué, E., Aragüés-Peñalba, M., and Gomis-Bellmunt, O. (2016). Topologies for large scale photovoltaic power plants. *Renewable and Sustainable Energy Reviews*, 59:309–319.

Chatterjee, A., Keyhani, A., and Kapoor, D. (2011). Identification of photovoltaic source models. *IEEE Transactions on Energy Conversion*, 26(3):883–889.

Comisión Reguladora de Energía (2006). Criteria of efficiency, quality, reliability, continuity, security and sustainability of the national electrical system: grid code (in spanish).

Comisión Reguladora de Energía (2016). Codigo de red.

De Brabandere, K., Bolsens, B., Van den Keybus, J., Woyte, A., Driesen, J., and Belmans, R. (2007). A voltage and frequency droop control method for parallel inverters. *IEEE Transactions on Power Electronics*, 22(4):1107–1115.

Ding, F., Nagarajan, A., Chakraborty, S., Baggu, M., Nguyen, A., Walinga, S., McCarty, M., and Bell, F. (2016). Photovoltaic impact assessment of smart inverter volt-var control on distribution system conservation voltage reduction and power quality. *National Renewable Energy Laboratory*.

Elrayyah, A., Sozer, Y., and Elbuluk, M. (2014). Modeling and control design of microgrid-connected pv-based sources. *IEEE Journal of Emerging and Selected Topics in Power Electronics*, 2(4):907–919.

Facchinei, F., Jiang, H., and Qi, L. (1999). A smoothing method for mathematical programs with equilibrium constraints. *Mathematical programming*, 85(1):107–134.

Fischer, A. (1992). A special newton-type optimization method. *Optimization*, 24(3-4):269–284.

Kamh, M. Z. and Iravani, R. (2012). Steady-state model and power-flow analysis of single-phase electronically coupled distributed energy resources. *IEEE Transactions on Power Delivery*, 27(1):131–139.

Kyocera (2014). Kyocera KU330-8BCA High efficiency multicrystal photovoltaic module.

Lim, L. H. I., Ye, Z., Ye, J., Yang, D., and Du, H. (2015). A linear identification of diode models from single i–v characteristics of pv panels. *IEEE Transactions on Industrial Electronics*, 62(7):4181–4193.

Mahmoud, Y. and El-Saadany, E. (2015). A photovoltaic model with reduced computational time. *IEEE Transactions on Industrial Electronics*, 62(6):3534–3544.

Mahmoud, Y., Xiao, W., and Zeineldin, H. (2012). A simple approach to modeling and simulation of photovoltaic modules. *IEEE Transactions on Sustainable Energy*, 3(1):185–186.

Milano, F. (2010). *Power system modelling and scripting*. Springer Science & Business Media.

Monteiro, L., Finelli, I., Quinan, A., Macêdo, W. N., Torres, P., Pinho, J. T., Nohme, E., Marciano, B., and Silva, S. R. (2016). Implementation and validation of energy conversion efficiency inverter models for small pv systems in the north of brazil. In *Renewable Energy in the Service of Mankind Vol II*, pages 93–102. Springer.

PRODESEN 2017 (2017). Development Program for the National Electrical System 2017-2031. Technical report, Secretaría de Energía.

Rampinelli, G., Krenzinger, A., and Romero, F. C. (2014). Mathematical models for efficiency of inverters used in grid connected photovoltaic systems. *Renewable and Sustainable Energy Reviews*, 34:578–587.

REMTF, W. (2010). Wecc power flow modeling guide for pv systems. Technical report.

Romero, A. M. (2014). Estabilidad de voltaje en redes con generación eólica. Master's thesis, Universidad Nacional Autónoma de México.

Rosehart, W., Roman, C., and Schellenberg, A. (2006). Optimal power flow with complementarity constraints. In *Power Systems Conference and Exposition, 2006. PSCE '06. 2006 IEEE PES*, pages 417–417.

Soto, W. D., Klein, S., and Beckman, W. (2006). Improvement and validation of a model for photovoltaic array performance. *Solar Energy*, 80(1):78 – 88.

Stijn, C. (2010). *Steady-state and dynamic modelling of VSC HVDC systems for power system Simulation*. PhD thesis, PhD dissertation, Katholieke University Leuven, Belgium.

Villalva, M., Gazoli, J., and Filho, E. (2009). Comprehensive approach to modeling and simulation of photovoltaic arrays. *IEEE Transactions on Power Electronics*, 24(5):1198–1208.

Xiao, W., Lind, M., Dunford, W., and Capel, A. (2006). Real-time identification of optimal operating points in photovoltaic power systems. *IEEE Transactions on Industrial Electronics*, 53(4):1017–1026.

Yi-Bo, W., Chun-Sheng, W., Hua, L., and Hong-Hua, X. (2008). Steady-state model and power flow analysis of grid-connected photovoltaic power system. In *2008 IEEE International Conference on Industrial Technology*, pages 1–6.

Zhang, X.-P. (2004). Multiterminal voltage-sourced converter-based hvdc models for power flow analysis. *IEEE Transactions on Power Systems*, 19(4):1877–1884.